Design, synthesis and biological evaluation of biphenyl-benzamides as potent FtsZ inhibitors

Deng, Jingjing; Zhang, Tao; Li, Baiqing; Xu, Mingyuan; Wang, Yuanze

Published in:
European Journal of Medicinal Chemistry

DOI:
10.1016/j.ejmech.2022.114553

Publication date:
2022

European Journal of Medicinal Chemistry 239 (2022) 114553

Contents lists available at ScienceDirect

European Journal of Medicinal Chemistry

journal homepage: www.elsevier.com/locate/ejmech

Design, synthesis and biological evaluation of biphenyl-benzamides as potent FtsZ inhibitors

Jingjing Deng [b], Tao Zhang [a], Baiqing Li [a], Mingyuan Xu [a], Yuanze Wang [a,*]

[a] Bioland Laboratory (Guangzhou Regenerative Medicine and Health - Guangdong Laboratory),Guangzhou, 510530, PR China
[b] Department of Molecular Genetics, University of Groningen, Groningen, Netherlands

ARTICLE INFO

Keywords:
Biphenyl-benzamide derivatives
FtsZ inhibitors
Antibacterial activity
Bacillus subtilis
Structure-based drug design

ABSTRACT

The rapid emergence of antibiotic resistance has become a prevalent threat to public health, thereby development of new antibacterial agents having novel mechanisms of action is in an urgent need. Targeting at the cytoskeletal cell division protein filamenting temperature-sensitive mutant Z (FtsZ) has been validated as an effective and promising approach for antibacterial drug discovery. In this study, a series of novel biphenyl-benzamides as FtsZ inhibitors has been rationally designed, synthesized and evaluated for their antibacterial activities against various Gram-positive bacteria strains. In particular, the most promising compound **30** exhibited excellent antibacterial activities, especially against four different *Bacillus subtilis* strains, with an MIC range of 0.008 μg/mL to 0.063 μg/mL. Moreover, compound **30** also showed good pharmaceutical properties with low cytotoxicity (CC_{50} > 20 μg/mL), excellent human metabolic stability ($T_{1/2}$ = 111.98 min), moderate pharmacokinetics ($T_{1/2}$ = 2.26 h, F = 61.2%) and *in vivo* efficacy, which can be identified as a promising FtsZ inhibitor worthy of further profiling.

1. Introduction

In recent years, the rapid emergence and increase of multidrug-resistant bacteria strains that resistance to current antibiotic therapy in both hospital and community has become a primary health problem for the whole world. Therefore, the need for discovery and development of new antimicrobial agents with novel mechanism of action has become increasingly urgent [1,2]. Cell division, also known as cytokinesis, is a crucial event for the survival of all bacterial cells and has been validated as one of the most promising targets to develop novel antibiotics [3,4]. In particular, filamenting temperature-sensitive mutant Z (FtsZ), a prokaryotic homolog of tubulin, is the most abundant and highly conserved cytoskeletal cell division protein in almost all bacteria. During the cell division process, the first step is the polymerization of FtsZ to form the Z ring in the midcell which used as the scaffold for the recruitment of dozens of other downstream cell division proteins [5–11]. Due to its essentiality for bacterial viability and high conservation among almost all the bacterial species, FtsZ has been widely explored and confirmed as an appealing target for antibacterial drug discovery [8–11].

The last decade has seen a surge in the publication of FtsZ inhibitors, most of which exert their antibacterial effect by binding to three identified pockets of FtsZ protein: the synergistic T7 loop, the nucleotide binding domain and the interdomain cleft [12–18]. Among them, the interdomain cleft has attracted extensive attention because this cavity is specific and not involved in any fundamental physiological function, thereby avoiding cross inhibition of tubulin and reducing the eukaryotic cell cytotoxicity. The most successful class of compounds targeting this pocket is benzamide anologs. Since the disclosure of the first hit compound 3-methoxy benzamide (3-MBA) [13], dozens of benzamide derivatives have been synthesized and identified as FtsZ inhibitors (Fig. 1). PC190723 is a milestone of these inhibitors with potent antibacterial activity despite its clinical development is obstructed by its poor pharmacokinetic property. Encouragingly, the prodrug of TXA707 (a PC190723 derivative) developed by Taxis pharmaceuticals, oral TXA709, has reached to phase I clinical trial for development as an anti-resistance drug to be used in combination with obsolete antibiotics as a fully oral anti-MRSA treatment.

It is well known that the biphenyl scaffold is a privileged moiety in drug design, especially for binding in the hydrophobic pocket of targets. The structure feature of the biphenyl core makes it possible to form strong hydrophobic interaction with the nearby residues. In addition, it

* Corresponding author.
E-mail address: wang_yuanze@grmh-gdl.cn (Y. Wang).

https://doi.org/10.1016/j.ejmech.2022.114553
Received 10 December 2021; Received in revised form 14 June 2022; Accepted 16 June 2022
Available online 21 June 2022

can also form pi-pi interactions with amino acids such as tyrosine and tryptophan. It has been successfully used in many marketed drugs, for example, anti-inflammatory drug Flurbiprofen, antifungal drug Bifonazole and antihypertensive drug Losartan (Fig. 2). Recently, biphenyl scaffold has also been used as the key pharmacophore of PD-L1 inhibitors (e.g., INCB084550) to block PD-1/PD-L1 protein-protein interaction which has been recognized as one of the most challenging drug discovery tasks because of the high-affinity interaction between two proteins [19].

3-(benzyloxy)-2,6-difluorobenzamide (**1**), a 3-MBA derivative, has been published as a FtsZ inhibitor with an MIC of 16 μg/mL against *B. subtilis* ATCC9372, 32 μg/mL against *S. aureus* ATCC25923 and 64 μg/mL against *S. aureus* ATCC29213 [20]. By docking of this hit compound with the FtsZ protein (RCSB: 3VOB) [21], we found that there is still a huge hydrophobic cavity lies toward C-3 position of the terminus benzene ring that could accommodate an extra aromatic group (Fig. 3). Therefore, a series of biphenyl-benzamide compounds was rationally designed, synthesized and evaluated for their antibacterial activities, cytotoxicity, docking studies, molecular dynamics, microsome stability and pharmacokinetics. In particular, one of the best compounds in this work, **30** showed 256–1000 times improvement than hit **1** in antibacterial activity with an MIC of 0.016 μg/mL against *B. subtilis* ATCC9372, 0.031 μg/mL against *B. subtilis* MG27, 0.008 μg/mL against *B. subtilis* 618, 0.016 μg/mL against *B. subtilis* BS01, 0.25 μg/mL against *S. aureus* ATCC29213 and 0.125 μg/mL against *S. aureus* ATCC25923.

2. Chemistry

The biphenyl-benzamide derivatives (**7–33**) were synthesized from the commercially available 2,4-difluoro-3-hydroxybenzoic acid (**2**) as outlined in Scheme 1. The alkylation of **2** with 3-bromobenzyl bromide **3** in the presence of sodium iodide and potassium carbonate produced intermediate **4.** Then the acid was converted to benzamide **6** using thionyl chloride, followed by treatment with ammonia carbonate. At last, the final products (**7–33**) were obtained by coupling of **6** with varies boronic acids (commercially available or made in house) in 73–89% yields.

For biphenyl-benzamide derivative **19a**, methyl 3-bromo-5-chlorobenzoate **36** was used as the starting material which first coupled with 4-trifluoromethylphenylboronic acid **37** to afford biphenyl intermediate **38**. Then the ester was reduced to hydroxyl group in the presence of $LiAlH_4$. After that, chlorination of **39** using thionyl chloride in DCM furnished intermediate **40** which reacted with **41** to give the desired compound **19a** (Scheme 2).

The synthetic route for compounds **19b** and **35a** is shown in Scheme 3. The biphenyl core was constructed by coupling of (3-bromophenyl) acetic acid methyl ester **42** with boronic acids. Then the intermediate **43** was brominated to give intermediate **44** using NBS and BPO. The alkylation of **41** with **44** in the presence of sodium carbonate produced intermediate **45**, which was further reduced by $LiAlH_4$ to yield the final products (**19b, 35a**).

3. Results and discussion

3.1. In vitro antibacterial activity of biphenyl-benzamide derivatives and SAR analysis

The target compounds listed in Table 1 were evaluated for their *in vitro* antibacterial activity by broth microdilution procedures described in the method recommended by the Clinical and Laboratory Standards Institute (CLSI) guidelines [22]. Preliminary minimal inhibitory concentration (MIC) values for all the target compounds were determined in comparison with compound **1**, PC190723 and vancomycin (Van) against penicillin-susceptible strain *B. subtilis* ATCC9372, penicillin-susceptible strain *S. aureus* ATCC25923, methicillin-resistance strain *S. aureus* ATCC29213.

To validate our design strategy based on the docking study, the simplest biphenyl-benzamide compound **7** was first synthesized as illustrated in Scheme 1. As expected, antibacterial results showed that the activity of **7** was significantly improved by replacement of the benzene ring with a biphenyl group. It showed an MIC of 0.5 μg/mL against *B. subtilis* ATCC9372, 2 μg/mL against *S. aureus* ATCC25923 and 2 μg/mL against *S. aureus* ATCC29213 (Table 1). Encouraged by these results, we then explored the preliminary SAR of the biphenyl-benzamide derivatives. A methyl group was first substituted to the C-4′, C-5′ and C-6′ position of the terminus benzene ring to explore the possible position for further optimization. Substitution at C-4′ position of the benzene ring (**8**) lead to a 2-fold improvement of antibacterial activity while substitution at C-5′ position (**9**) is detrimental to the activity. To our delight, C-6′ was found to be the optimal position for further explore as compound **10** exhibited 4-fold improvement of activity against all three bacteria strains compared with compound **7**. Therefore, different types of functional groups were substituted at C-6′ position. Extension the length of the alkyl chain from methyl group to n-butyl group (**11**–**13**) has little impact on the antibacterial activity but n-pentyl group and bulky alkyl groups such as isopropyl and *tert*-butyl group resulted in complete loss of the activity against *S. aureus*. In addition, several election withdrawing groups were also explored at C-6' position (**17**–**21**). The cyano group, although known as a privileged scaffold to improve the drug-like property of the compound, also lead to a complete loss of the antibacterial activity (**18**). Interestingly, fluorine and trifluoromethyl substitution (**19**, **20**) exhibited exactly the same activity against all three bacterial strains. The most potent compound (**21**) showed an MIC of 0.063 μg/mL against *B. subtilis* ATCC9372, 0.25 μg/mL against *S. aureus* ATCC25923 and 0.25 μg/mL against *S. aureus* ATCC29213. Besides, the effect of the halogen substitutions at C-4 position of the biphenyl core was also explored. A 4-chloro substituted derivative **19a** was synthesized according to Scheme 2, but it failed to further improve the antibacterial activity of compound **19**.

Subsequently, a series of biphenyl-benzamide derivatives with di-substitution at the terminus benzene ring was explored. Similar to compound with C-5′ mono-substitution (**9**), C-5′ and C-6′ di-substitution (**22**, **23**) absolutely abolished their antibacterial activity with an MIC more than 128 μg/mL in all three strains. Encouragingly, C-4′ and C-6′ di-substitution (**24**–**33**) showed generally excellent antibacterial activity. When trifluoromethyl group was substituted at C-6′ position, six compounds were synthesized and evaluated. Among them, compounds **25** and **27** exhibited exactly the same activity with an MIC of 0.031 μg/mL against *B. subtilis* ATCC9372 and 0.25 μg/mL against *S. aureus* ATCC25923 and *S. aureus* ATCC29213. Unexpectedly, the antibacterial activity is completely lost when amide group was substituted at C-4' position (**26**), probably due to its high steric hindrance. In particular, compound **30** showed the most potent activity with an MIC of 0.016 μg/mL against *B. subtilis* ATCC9372, 0.125 μg/mL against *S. aureus* ATCC25923 and 0.25 μg/mL against *S. aureus* ATCC29213. Moreover, introducing a methyl or hydroxymethyl group at the ether linker has

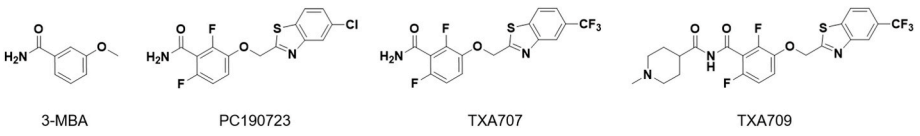

Fig. 1. Selected examples of benzamide derivatives as FtsZ inhibitors.

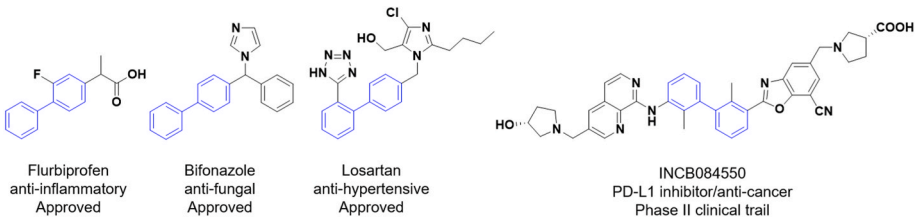

Fig. 2. Selected examples of clinical or approved drugs with biphenyl scaffold.

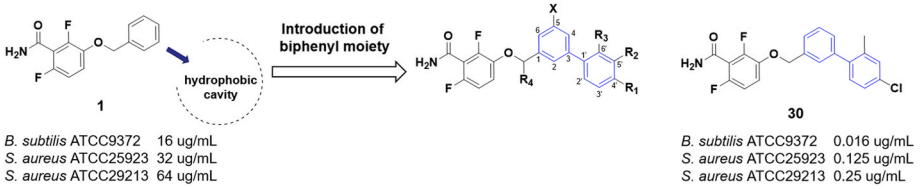

Fig. 3. Rational design of biphenyl-benzamide FtsZ inhibitors.

Table 1
In vitro antibacterial activity of the target compounds.

Compds	R_1	R_2	R_3	*B. subtilis* ATCC9372 (μg/mL)	*S. aureus* ATCC29213 (μg/mL)	*S. aureus* ATCC25923 (μg/mL)
7	-H	-H	-H	0.5	2	2
8	-H	-H	$-CH_3$	0.25	1	1
9	-H	$-CH_3$	-H	32	>128	>128
10	$-CH_3$	-H	-H	0.125	0.5	0.5
11	CH_2CH_3	-H	-H	0.125	0.5	0.5
12	$-CH_2CH_2CH_3$	-H	-H	0.125	1	1
13	$-CH_2(CH_2)_2CH_3$	-H	-H	0.125	1	0.5
14	$-CH_2(CH_2)_3CH_3$	-H	-H	0.125	>128	>128
15	$-CH_2(CH_3)_2$	-H	-H	0.5	>128	>128
16	$-CH(CH_3)_3$	-H	-H	2	>128	>128
17	$-OCH_3$	-H	-H	0.25	2	1
18	-CN	-H	-H	>128	>128	>128
19	$-CF_3$	-H	-H	0.125	2	1
19a	–	–	–	1	>128	>128
20	-F	-H	-H	0.125	2	1
21	-Cl	-H	-H	0.063	0.25	0.25
22	$-CF_3$	-F	-H	>128	>128	>128
23	$-CF_3$	-Cl	-H	>128	>128	>128
24	$-CF_3$	-H	$-OCH_3$	0.063	1	1
25	$-CF_3$	-H	$-CH_3$	0.031	0.25	0.25
26	$-CF_3$	-H	$-CONH_2$	>128	>128	>128
27	$-CF_3$	-H	-Cl	0.031	0.25	0.25
28	$-CF_3$	-H	-F	0.063	1	1
29	$-CF_3$	-H	$-CF_3$	0.125	0.5	0.5
30	-Cl	-H	$-CH_3$	0.016	0.25	0.125
31	-Cl	-H	-Cl	0.031	0.25	0.25
32	-Cl	-H	-F	0.016	0.5	0.5
33	-Cl	-H	$-CF_3$	0.125	0.5	0.5
19b	$-CF_3$	-H	-H	0.5	8	4
30a	-Cl	-H	$-CH_3$	0.125	1	1
1	–	–	–	16	64	32
VAN	–	–	–	1	1	0.5
PC190723	–	–	–	0.5	1	1

VAN: Vancomycin.

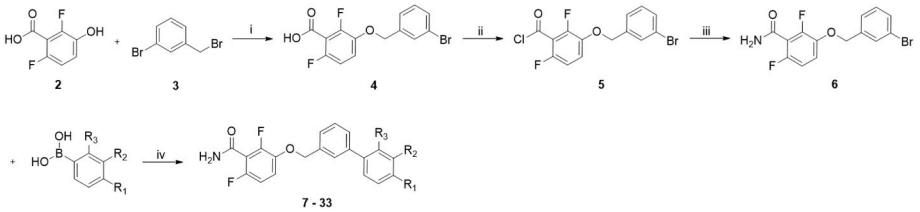

Scheme 1. Synthetic route for compounds **7**–**33**. Reagents and conditions: (i) K_2CO_3, KI, DMF, 50 °C; (ii) oxalyl chloride, DMF, DCM, r.t.; (iii) ammonium carbonate, DCM, rt; (iv) $Pd(dppf)Cl_2$, Na_2CO_3, dioxane/H_2O, 100 °C.

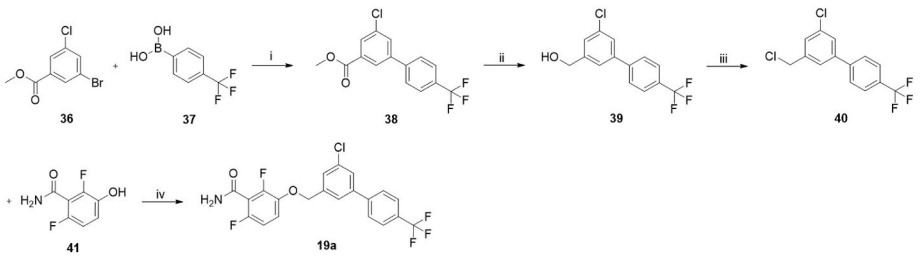

Scheme 2. Synthetic route for compound **19a**. Reagents and conditions: (i) $Pd(dppf)Cl_2$, Na_2CO_3, dioxane/H_2O, 100 °C; (ii) $LiAlH_4$, THF, 0 °C; (iii) thionyl chloride, DCM, 40 °C; (iv) K_2CO_3, KI, DMF, 50 °C.

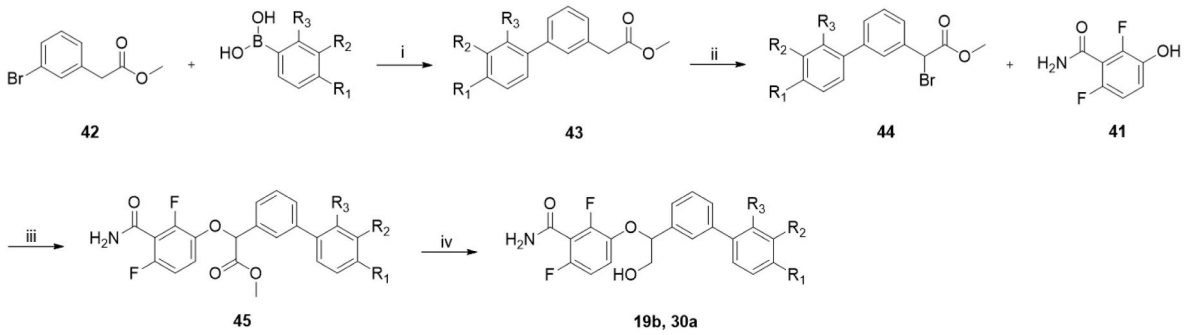

Scheme 3. Synthetic route for compounds **19b** and **30a**. Reagents and conditions: (i) $Pd(dppf)Cl_2$, Na_2CO_3, dioxane/H_2O, 100 °C; (ii) NBS, BPO, $CHCl_3$, reflux; (iii) Na_2CO_3, DMF; (iv) $LiAlH_4$, THF/MeOH.

been reported to improve the activity of FtsZ inhibitors [23]. Therefore, compounds **19b** and **30a** were synthesized as shown in Scheme 3. However, both of their antibacterial activities were slightly reduced compared with their parent compounds.

As several biphenyl-benzamide derivatives displayed remarkable antibacterial activities against *B. subtilis* ATCC9372, we further determined the activity of compounds **25**, **27**, **30** and **32** against another three *B. subtilis* strains. As shown in Table 2, these compounds showed excellent activity against all these strains with an MIC range of 0.008 μg/mL to 0.063 μg/mL. Compound **30** still exhibited the best activity with an MIC of 0.031 μg/mL against *B. subtilis* MG27, 0.008 μg/mL against *B. subtilis* 618 and 0.016 μg/mL against *B. subtilis* BS01. In addition, compound **30** was also evaluated in a variety of different pathogenic bacteria, including sensitive and resistant strains of Gram-positive and Gram-negative bacteria and it did not show antibacterial activity against Gram-negative bacteria strains (Table 3).

3.2. Cytotoxicity against Vero cells and selectivity index (SI) of selected compounds

With the antibacterial activities of biphenyl-benzamide compounds in hand, the cytotoxicity of compounds **25**, **27**, **30** and **32** were further tested against African green monkey kidney cells (Vero cells) using the Alamar blue assay (Table 4). The 50% cytotoxic concentration (CC_{50}) is defined as the lowest concentration of compound which leads to a 50% reduction in cell viability. The results indicated that all of these compounds are nontoxic to Vero cells (CC_{50} > 20 μg/mL) and exhibited favorable selectivity index (SI) larger than 645, indicating that these compounds are generally safe toward mammalian cells.

Table 2
In vitro antibacterial activity of compounds **25**, **27**, **30** and **32** against four different *B. subtilis* strains.

Compds	*B. subtilis* ATCC9372 (μg/mL)>	*B. subtilis* MG27 (μg/mL)	*B. subtilis* 618 (μg/mL	*B. subtilis* BS01 (μg/mL)
25	0.031	0.063	0.031	0.016
27	0.031	0.063	0.063	0.031
30	0.016	0.031	0.008	0.016
32	0.016	0.031	0.016	0.016

3.3. Bactericidal or bacteriostatic assay

Encouraged by its potent antibacterial activity and low cytotoxicity, the MBC of compound **30** was further determined against *S. aureus* ATCC25923 and *B. subtilis* ATCC9372 to investigate whether its activity was bactericidal or bacteriostatic. According to the CLSI standards, a bactericidal antibiotic has an MBC to MIC ratio of ≤4, while a bacteriostatic agent has an MBC to MIC ratio of >4. The results summarized in Table 5 showed that compound **30** exhibited an MBC/MIC ratio of 2 against *S. aureus* ATCC25923 and an MBC/MIC ratio of 4 against *B. subtilis* ATCC9372, which was regarded as bactericidal behavior.

3.4. Kinetics of the bactericidal activity and bacteria resistance evaluation

To further investigate the antibacterial activity of the newly synthesized biphenyl-benzamide compounds, the time-killing curve determinations were performed to explore the antibacterial kinetics of compound **30** against *S. aureus* ATCC25923 and *B. subtilis* ATCC9372. The experiment was performed as previously reported [22] and the results are presented in Fig. 4. The bacteria showed no reduction in the counts of CFU from vehicle which was incubated without compound **30**. Fig. 4A showed that 4 × MIC concentration of compound **30** can rapidly cause a reduction of *S. aureus* ATCC25923 below the lowest detectable limit (10^3 CFU/mL) in 3 h. The growth of *S. aureus* ATCC25923 can be completely inhibited in all the concentrations after 12 h. For *B. subtilis* ATCC9372 bacteria survival assay, 2 × MIC of compound **30** can reduce the viable counts below the lowest detectable limit after incubation for 3 h (Fig. 4B). These results revealed that biphenyl-benzamide derivatives can inhibit the bacteria growth quickly in a bactericidal mode. In addition, the multipassage resistance selection assay was used to evaluate the potential resistance development of compound **30**. *S. aureus*

Table 3
In vitro antibacterial activity of compound **30** against sensitive and resistant strains of Gram-positive and Gram-negative bacteria.

Compds	*S. aureus* 669[a] (μg/mL)	*S. aureus* 6917[a,b] (μg/mL)	*S. aureus* shhsE1[c] (μg/mL)	*E. coli* 25922 (μg/mL)	*P.aeruginosa* 15690 (μg/mL)	*K.pneumoniae* 14578 (μg/mL)
30	0.06	0.125	0.125	>128	>128	>128
VAN	0.5	0.5	0.5	>128	>128	>128

[a] Ampicillin-resistant strain.
[b] Kanamycin-resistant strain.
[c] Methicillin-resistant strain; VAN: Vancomycin.

Table 4
Cytotoxicity profile against Vero cells and Selectivity Index (SI).

No.	Compds	*B. subtilis* ATCC9372 (μg/mL)	CC_{50} against Vero cells (μg/mL)	Selectivity Index (CC_{50}/MIC)
1	**25**	0.031	>20	>1250
2	**27**			
3	**30**	0.016	>20	>645
4	**32**			

Table 5
Comparison of MBC and MIC of compound **30** against two bacteria strains.

Bacteria strains	Compds	MBC (μg/mL)	MIC (μg/mL)	MBC/MIC
S. aureus ATCC25923	**30**	0.25	0.125	2
	Vancomycin	0.5	0.5	1
B. subtilis ATCC9372	**30**	0.063	0.016	4
	Vancomycin	1	1	1

ATCC29213 was passaged for 18 cycles at subinhibitory concentration (0.5 × MIC) of **30** and norfloxacin. As shown in Fig. 5, only 4-fold MIC increase was observed for compound **30** after 18 passages, while the MIC of norfloxacin was increased by 128-fold. These results indicated that compound **30** avert the bacterial resistance and could represent as a potential candidate to combat drug-resistant bacteria.

3.5. Effects on the FtsZ polymerization and GTPase activity

The effect of compound **30** on polymerization of *Sa*FtsZ was first visualized by transmission electron microscopy (TEM). It was found that the size and thickness of the *Sa*FtsZ polymer was substantially increased after treatment with 10 μg/mL of compound **30**, indicating that this compound could stimulate the bundling of the FtsZ protofilaments (Fig. 6). To further validate this phenomenon, a microliter plate-based spectrophotometric light-scattering approach was conducted to detect FtsZ polymerization by measuring the solution absorbance at 340 nm. As shown in Fig. 7A, 10 μg/mL of compound **30** was able to significantly induce the polymerization of *Sa*FtsZ. Moreover, it could also effectively inhibit the GTPase activity of *Sa*FtsZ in a dose-dependent manner (Fig. 7B).

3.6. Effects on the morphology of Bacillus subtilis

FtsZ inhibitors are well known to disrupt bacterial cell division and change the morphology of bacteria. Thus, *B. subtilis* ATCC9372 was incubated with compound **30** at 1 × MIC concentration and their morphology was observed through an optical microscope. The results showed that the length of the *B. subtilis* ATCC9372 was much longer than the control. As shown in Fig. 8, the length of *B. subtilis* ATCC9372 control cells was around 10 μm, while the cells treated with compound **30** were found longer than 60 μm. These results strongly suggested that our biphenyl-benzamide derivatives can cause abnormal bacterial cell division and lead to bacterial cell death, which is consistent with the previously reported benzamide inhibitors targeted on FtsZ [24,25].

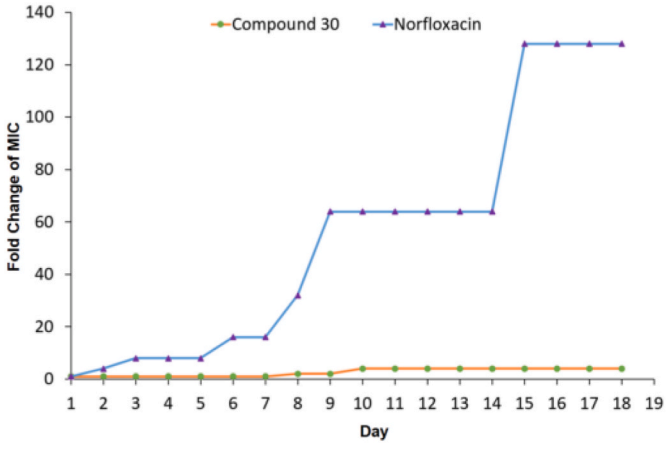

Fig. 5. Propensity of development of bacterial resistance against compound **30**.

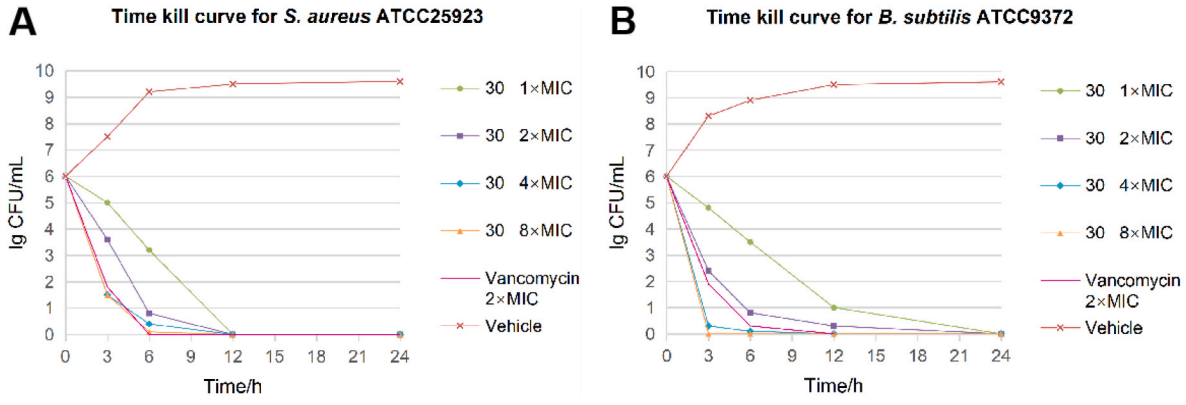

Fig. 4. Time kill curve of compound **30** against two bacteria strains.

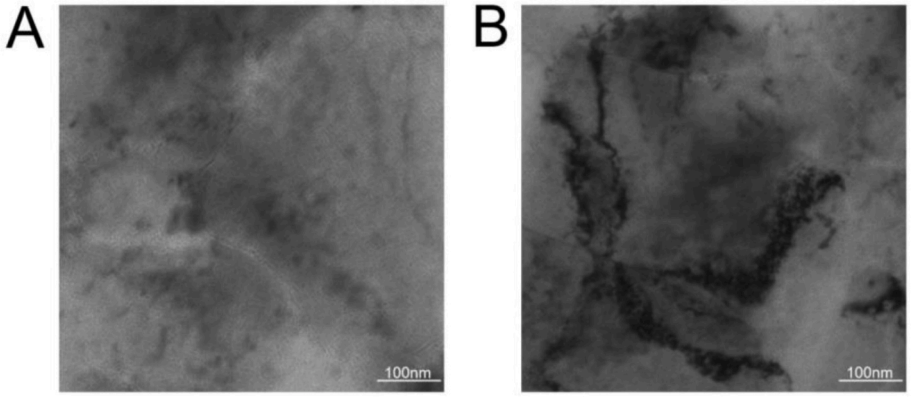

Fig. 6. Transmission electron micrographs of *Sa*FtsZ polymers in the presence of DMSO vehicle (A) and in the presence of compound **30** (B) at 10 μg/mL.

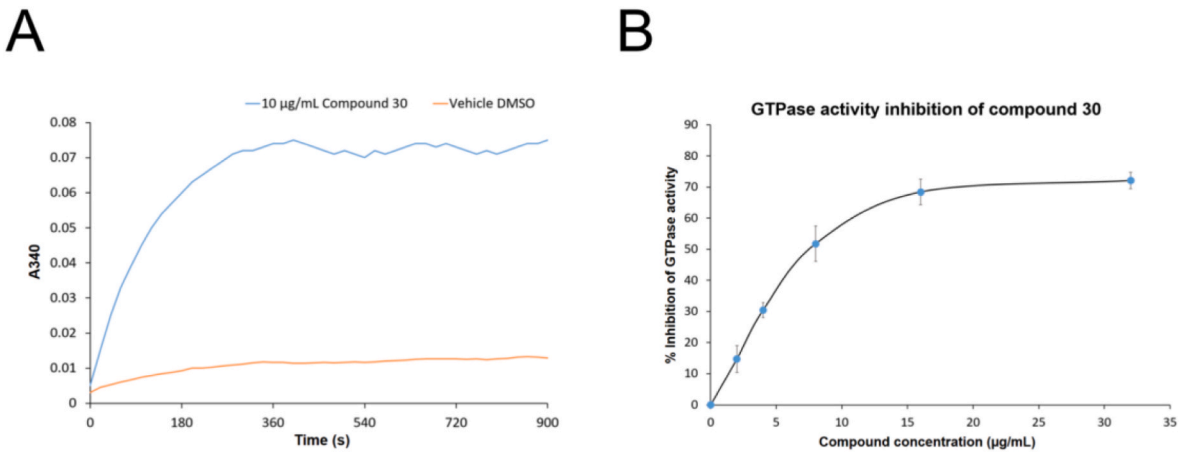

Fig. 7. (A) The impact of compound **30** on the polymerization of *Sa*FtsZ in a concentration-dependent manner; (B) Inhibition of GTPase activity of *Sa*FtsZ by different concentrations of compound **30**.

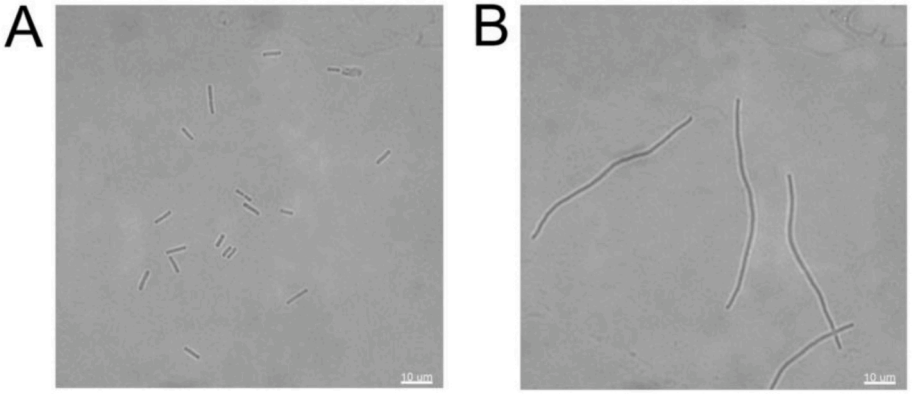

Fig. 8. Morphology of *B. subtilis* ATCC9372 in the absence or presence of compound **30** (0.016 μg/mL).

3.7. Computational studies of the binding mode and molecular dynamics (MD) simulation

The computational analysis of compound **30** with SaFtsZ protein was evaluated by induced fit docking (IFD) module of Schrödinger. As shown in Fig. 9, compound **30** adopts an ideal conformation in the hydrophobic pocket (PC-site) near the T7 loop. Similar to PC190723, the benzamide moiety of compound **30** makes three key interactions with SaFtsZ. The carbonyl group of the benzamide coordinated with the calcium ion and the primary amino group forms two hydrogen bond with the carbonyl of Val207 and Asn263. Two fluoro groups at the ortho position of the amide are located in hydrophobic cores generated by residues Leu200, Val203, Leu209 and Leu297. The ether linker function as an adjusting spacer that properly places the biphenyl moiety in the hydrophobic cavity formed by amino-acid residues Gln192, Gly193, Gly196, Leu200, Met226, Thr309, Val310 and Ile311. In addition, an electrostatic interaction is formed between the terminus chloro group in biphenyl moiety and the amide hydrogen in the side chain of Gln192.

Subsequently, the dynamics of compound **30** and protein complex system was evaluated by MD simulation. 100ns NPT MD simulations is

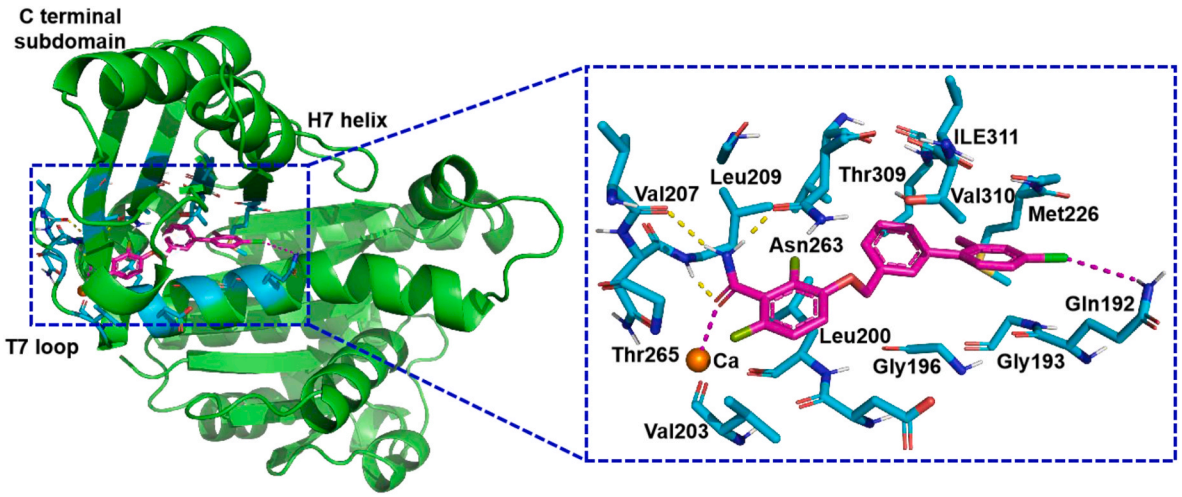

Fig. 9. Predicted binding modes of SaFtsZ (PDB ID: 3vob) in complex with compound **30**.

performed in a TIP3P explicit water box with a radius of 20 Å and the values of root mean square deviation (RMSD) were calculated to analyze the overall structure stability and conformational changes. As shown in Fig. 10A, there are sharply increase during 0–5 ns in both complex systems. In particular, the RMSD values of compound **30**-FtsZ complex is similar to **PC190723**-FtsZ complex after 10 ns, which indicate both systems have comparable stability. In addition, the RMSD values of key amino acids around the binding pocket of compound **30** and PC190723 were also compared (Fig. 10B). Obviously, these amino acid residues fluctuated significantly in both systems before 30 ns, probably because initial binding of the ligands tended to change the flexibility of amino acids around the pocket. Similarly, both systems leveled off in the last 70 ns and finally reached to a relatively stable state.

3.8. Microsome stability on mouse, rat and human

Metabolic stability is a key parameter in defining the pharmacological and toxicological profile of drugs as well as patient compliance during the drug discovery and development process. Therefore, compound **30** was further evaluated for *in vitro* metabolic stability in mouse, rat and human liver microsomes. Ketanserin was used as the reference compound for the microsome stability experiment. As shown in Table 6, compound **30** shows great difference among these species. It disappears rapidly in mouse and rat liver microsomes with a half-life of 5.09 and 13.55 min, respectively. Fortunately, it is more stable in human liver microsome with a half-life of 111.98 min and low clearance of 15.52 mL/min/kg.

3.9. Pharmacokinetics and in vivo efficacy

With its excellent *in vitro* antibacterial potency and favorable microsome stability profile, compound **30** was further progressed into *in vivo* pharmacokinetic studies at an intravenous dose of 1 mg/kg and at an oral dose of 5 mg/kg in ICR mouse. As illustrated in Table 7, the plasma PK of compound **30** via intravenous (iv) route at 1 mg/kg dose revealed its high clearance at 5682.8 mL/h/kg with short terminal half-life ($t_{1/2}$) of 0.28 h. It is well known that the benzamide FtsZ inhibitors such as PC190723 have suffered from poor pharmacokinetic property and the prodrug strategy has been developed. To our delight, it exhibited moderate exposure ($AUC_{(0\text{-}t)}$ = 544.2 h*ng/mL) for oral administration of compound **30** at 5 mg/kg dose with an oral bioavailability (F) of 61.2%. In addition, compound **30** was preliminarily assessed for *in vivo* efficacy using a mouse blood model of infection. In brief, the mice divided into three group (four mice per group) were infected with about 6×10^6 CFUs of *S. aureus* ATCC25923 for 1h, followed by treatment with 0.5 mL saline (negative control), 0.5 mL compound **30** (25 mg/kg), and 0.5 mL vancomycin (25 mg/kg), respectively. As shown in Fig. 11, compound **30** significantly reduced the bacteria burden and showed

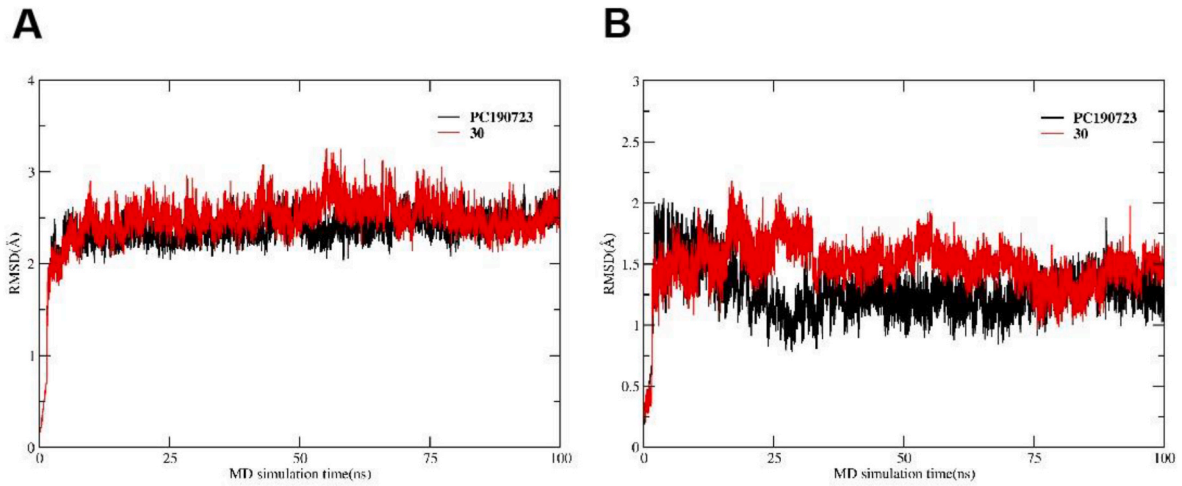

Fig. 10. (A) RMSD values of the overal **30**-FtsZ and **PC190723**-FtsZ complex systems. (B) RMSD values of key amino acids around the binding pocket in both systems.

Table 6
Stability of compound **30** in mouse, rat and human liver microsomes.

Test Article	Species		Percent Remaining (%)					$T_{1/2}$ (minute)	Cl_{int} (mL/min/kg)
			0 min	5 min	15 min	30 min	45 min		
Ketanserin	human	Mean	100.00	81.82	64.17	48.64	34.28	30.45	57.09
		RSD[a]	0.02	0.00	0.02	0.01	0.01		
	rat	Mean	100.00	76.92	45.05	20.58	12.06	14.49	171.42
		RSD[a]	0.06	0.03	0.03	0.05	0.12		
	mouse	Mean	100.00	63.78	25.05	7.84	2.62	8.57	637.04
		RSD[a]	0.03	0.01	0.02	0.01	0.09		
30	human	Mean	100.00	97.08	86.18	83.41	74.96	111.98	15.52
		RSD[a]	0.02	0.01	0.03	0.02	0.06		
	rat	Mean	100.00	73.71	39.02	19.07	10.00	13.55	183.28
		RSD[a]	0.01	0.03	0.03	0.05	0.03		
	mouse	Mean	100.00	53.10	11.94	1.74	0.46	5.09	1072.34
		RSD[a]	0.01	0.09	0.08	0.02	0.44		

[a] Relative Standard Deviation of Area Ratio.

Table 7
Murine pharmacokinetic profiles of compound **30**.

No.	Route	Dose (mg/kg)	$T_{1/2}$ (h)	T_{max} (h)	C_{max} (ng/mL)	$AUC_{(0\text{-}t)}$ (h*ng/mL)	$AUC_{(0\text{-}\infty)}$ (h*ng/mL)	V_{ss} (ng/mL)	CL (mL/h/kg)	F %
30	IV[a,c]	1	0.28	0.083	480.5	177.8	178.7	1545.5	5682.8	/
	PO[b,c]	5	2.26	0.5	429.3	544.2	559.3	/	/	61.2

[a] Three mice per study for IV.
[b] Three mice per study for PO.
[c] Formulation: 5% DMSO/4% ethanol/5% Cremophor EL/86% water.

comparable *in vivo* efficacy with vancomycin.

4. Conclusion

In conclusion, based on the docking studies of hit compound **1**, a series of novel biphenyl-benzamide derivatives have been rationally designed, synthesized and evaluated against various gram-positive bacteria strains. The results indicate that these compounds exhibit significant antibacterial activity against most of the testing strains. Among them, the most potent compound **30** displayed antibacterial activities against various *S. aureus* and *B. subtilis* with an MIC ranging from 0.008 μg/mL to 0.25 μg/mL. It is noteworthy that the activities of compound **30** were significantly improved compared with the hit compound **1** and even much better than PC190723 and vancomycin. In bactericidal kinetic assay, compound **30** was found to have rapid bactericidal properties which can rapidly cause a reduction of *S. aureus* ATCC25923 and *B. subtilis* ATCC9372 cells below the lowest detectable limit (10^3 CFU/mL) in 3 h at 4 × MIC concentration. Inverted fluorescence microscopy analysis revealed the extension of *B. subtilis* length with compound **30** suggesting that it has the same mechanism of action as previously reported FtsZ targeting benzamide derivatives. In addition, compound **30** was found to be non-toxic to Vero cells ($CC_{50} > 20$ μg/mL) and exhibited favorable selectivity index. Moreover, compound **30** also showed good pharmaceutical properties with excellent human metabolic stability ($T_{1/2} = 111.98$ min), moderate pharmacokinetics ($T_{1/2} = 2.26$ h, F = 61.2%) and *in vivo* efficacy. All together, the studies described herein highlight compound **30** as a lead compound targeting FtsZ with excellent antibacterial activities and pharmaceutical properties. Further optimization of the drug-like property and *in vivo* studies of the biphenyl-benzamide derivatives are ongoing in our lab.

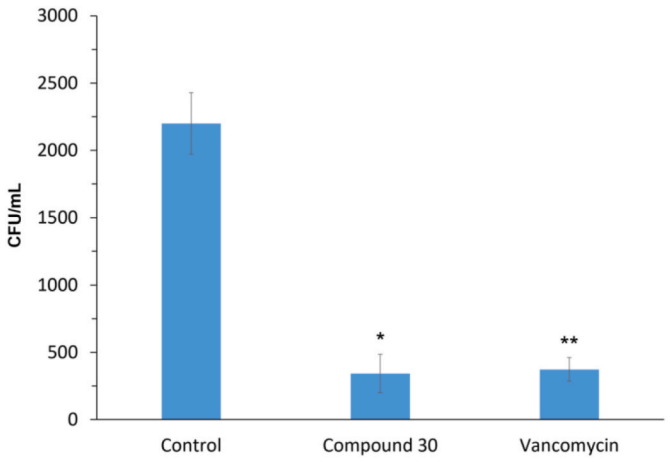

Fig. 11. *In vivo* efficacy of compound **30** and vancomycin in a mouse blood model of infection with *S. aureus* ATCC25923.*P < 0.01, **P < 0.005, compared with the negative control group.

5. Experiment section

All reagents and solvents were purchased from commercial suppliers and used without any purification unless otherwise noted. The product solutions were evaporated *in vacuo* using a rotatory evaporator. The reactions were monitored by thin layer chromatography (TLC) using GF254 silica gel plates visualized with ultraviolet (UV) light (254 nm). Flash chromatography was performed using RediSep Rf Normalphase Silica Flash Columns (Silica Gel 60 Å, 230–400 mesh). Nuclear magnetic resonance spectra (NMR) were recorded on a Bruker Avance 500 spectrometer (^{1}H NMR (500 MHz), ^{13}C NMR (101 MHz)). Chemical shifts for ^{1}H NMR were reported as δ values and coupling constants were in hertz (Hz). The following abbreviations were used for spin multiplicity: s = singlet, bs = broad singlet, d = doublet, t = triplet, q = quartet, m = multiplet. Chemical shifts for ^{13}C NMR reported in ppm relative to the solvent peak. Low-resolution mass spectra (MS) and compound purity data were acquired on a Waters ZQ LC/MS single quadruped system equipped with an electrospray ionization (ESI) source, a UV detector (220 nm and 254 nm), and an evaporative light scattering detector (ELSD). High resolution mass spectra were recorded using an LTQ-Orbitrap-XL (Thermo Fisher Scientific; ESI+ mode) at a resolution of 60000@*m/z*400. High performance liquid chromatography (HPLC) analysis revealed a purity of >95% for all compounds.

5.1. Synthesis

5.1.1. 3-((3-bromobenzyl)oxy)-2,6-difluorobenzoic acid (4)

To a solution of 2,4-difluorophenol **2** (3.0 g, 17.2 mmol) in THF (20 mL) was added NaOH (43 mL, 1 M, 43.1 mmol), 1-bromo-3-(bromomethyl)benzene **3** (9.0 g, 3.6 mmol) at 0 °C and stirred for 1 h. Then the resulting solution was heated to reflux and stirred overnight. The mixture was acidified by HCl solution (1 M) and filtrated. The filter cake was dissolved in DCM and purified by flash column chromatography (DCM/MeOH, 97/3) to yield the intermediate **4** (4.6 g, 77.9%). ESI-MS calcd. for $C_4H_9BrF_2O_3$ $[M + H]^+$, 343.0, found 343.1.

5.1.2. 3-((3-bromobenzyl)oxy)-2,6-difluorobenzamide (6)

To a solution of **4** (4.6 g, 13.4 mmol) in DCM (60 mL) was added oxalyl chloride (1.8 mL, 1.5 g/mL, 20.1 mmol) at 0 °C and stirred at room temperature for 3 h. The resulting solution was evaporated to yield the crude intermediate **5** as yellowish liquid. Then crude intermediate **5** was dissolved in DCM (100 mL) and ammonium carbonate (4.0 g, 22.8 mmol) was added. The resulting solution was stirred at room temperature for 15 h. The mixture was added MeOH (5 mL), filtered and washed with MeOH. The filtrate was evaporated and purified by flash column chromatography (DCM/MeOH, 20/1) to yield the intermediate **6** (4.3 g, 93.8%). ESI-MS calcd. for $C_{14}H_{10}BrF_2NO_2$ $[M + H]^+$, 342.0, found 342.1.

5.1.3. Typical procedure for the synthesis of (7–33)

To a solution of **6** (100 mg, 0.29 mmol) in dioxane (3 mL) and H_2O (0.5 mL) was added boric acid (0.35 mmol), $Pd(dppf)Cl_2$ (42.4 mg, 0.06 mmol), Na_2CO_3 (92.2 mg, 0.87 mmol) and heated with microwave at 100 °C for 1 h. The reaction mixture was diluted with EtOAc (25 mL), washed with H_2O, washed with brine and dried over Na_2SO_4. The resulting solution was evaporated and purified by flash column chromatography (PE/EA, 70/30) to afford the according products in good yield.

Synthesis of 3-([1,1′-biphenyl]-3-ylmethoxy)-2,6-difluorobenzamide (7): white solid, 86.3% yield; HPLC purity: 99.2%; ^{1}H NMR (500 MHz, DMSO) δ 8.13 (s, 1H), 7.84 (s, 1H), 7.75 (s, 1H), 7.66 (t, J = 9.7 Hz, 3H), 7.53–7.43 (m, 4H), 7.41–7.29 (m, 2H), 7.07 (t, J = 8.8 Hz, 1H), 5.26 (s, 2H); ^{13}C NMR (101 MHz, DMSO) δ 161.3, 153.1, 150.7, 149.3, 146.8, 142.8, 140.4, 139.8, 137.1, 129.2, 129.0, 127.6, 126.9, 126.7, 126.5, 126.2, 116.0, 111.0, 110.8, 70.8. HRMS (ESI) calcd. for $C_{20}H_{15}F_2NO_2$ $[M + H]^+$, 340.1104, found 340.1141.

Synthesis of 2,6-difluoro-3-((2′-methyl-[1,1′-biphenyl]-3-yl)methoxy)benzamide (8): white solid, 86.7% yield; HPLC purity: 100%; ^{1}H NMR (500 MHz, DMSO) δ 8.12 (s, 1H), 7.83 (s, 1H), 7.50–7.39 (m, 3H), 7.35–7.23 (m, 5H), 7.20 (d, J = 6.1 Hz, 1H), 7.07 (t, J = 8.9 Hz, 1H), 5.24 (s, 2H), 2.21 (s, 3H); ^{13}C NMR (101 MHz, DMSO) δ 161.3, 153.1, 150.7, 149.4, 146.9, 142.8, 141.4, 140.9, 136.3, 134.7, 130.4, 129.5, 128.7, 128.5, 127.5, 126.4, 126.0, 115.9, 116.0, 70.8, 21.1. HRMS (ESI) calcd. for $C_{21}H_{17}F_2NO_2$ $[M + H]^+$, 354.1261, found 354.1308.

Synthesis of 2,6-difluoro-3-((3′-methyl-[1,1′-biphenyl]-3-yl)methoxy)benzamide (9): white solid, 81.5% yield; HPLC purity: 99.3%; ^{1}H NMR (500 MHz, DMSO) δ 8.13 (s, 1H), 7.84 (s, 1H), 7.73 (s, 1H), 7.63 (d, J = 7.6 Hz, 1H), 7.52–7.41 (m, 4H), 7.39–7.28 (m, 2H), 7.20 (d, J = 7.4 Hz, 1H), 7.07 (t, J = 8.9 Hz, 1H), 5.26 (s, 2H), 2.38 (s, 3H); ^{13}C NMR (101 MHz, DMSO) δ 161.3, 153.1, 150.7, 149.3, 146.9, 142.7, 140.5, 139.8, 138.1, 137.0, 129.2, 128.9, 128.3, 127.4, 126.8, 126.2, 123.8, 115.9, 111.0, 70.8, 21.1. HRMS (ESI) calcd. for $C_{21}H_{17}F_2NO_2$ $[M + H]^+$, 354.1261, found 354.1309.

Synthesis of 2,6-difluoro-3-((4′-methyl-[1,1′-biphenyl]-3-yl)methoxy)benzamide (10): white solid, 89.0% yield; HPLC purity: 100%; ^{1}H NMR (500 MHz, DMSO) δ 8.12 (s, 1H), 7.84 (s, 1H), 7.72 (s, 1H), 7.62 (d, J = 7.7 Hz, 1H), 7.56 (d, J = 8.0 Hz, 2H), 7.48 (t, J = 7.6 Hz, 1H), 7.41 (d, J = 7.6 Hz, 1H), 7.35–7.26 (m, 3H), 7.07 (t, J = 8.6 Hz, 1H), 5.25 (s, 2H), 2.35 (s, 3H); ^{13}C NMR (101 MHz, DMSO) δ 161.3, 153.0, 150.6, 149.3, 146.9, 142.8, 142.7, 140.3, 137.0, 136.9, 129.6, 129.2, 126.6, 126.5, 126.2, 125.9, 115.9, 111.0, 110.8, 70.8, 20.7. HRMS (ESI) calcd. for $C_{21}H_{17}F_2NO_2$ $[M + H]^+$, 354.1261, found 354.1285.

Synthesis of 3-((4′-ethyl-[1,1′-biphenyl]-3-yl)methoxy)-2,6-difluorobenzamide (11): white solid, 83.5% yield; HPLC purity: 98.2%; ^{1}H NMR (500 MHz, DMSO) δ 8.13 (s, 1H), 7.84 (s, 1H), 7.72 (s, 1H), 7.64–7.56 (m, 3H), 7.48 (t, J = 7.6 Hz, 1H), 7.42 (d, J = 7.6 Hz, 1H), 7.35–7.29 (m, 3H), 7.07 (t, J = 8.5 Hz, 1H), 5.25 (s, 2H), 2.65 (q, J = 7.6 Hz, 2H), 1.27–1.18 (m, 4H); ^{13}C NMR (101 MHz, DMSO) δ 161.3, 153.1, 150.7, 149.3, 146.8, 143.3, 142.8, 140.4, 137.2, 137.0, 129.2, 128.4, 126.6, 126.6, 126.3, 126.0, 115.9, 111.0, 110.8, 70.8, 27.8, 15.6. HRMS (ESI) calcd. for $C_{22}H_{19}F_2NO_2$ $[M + H]^+$, 368.1417, found 368.1460.

Synthesis of 2,6-difluoro-3-((4′-propyl-[1,1′-biphenyl]-3-yl)methoxy)benzamide (12): white solid, 82.4% yield; HPLC purity: 100%; ^{1}H NMR (500 MHz, DMSO) δ 8.13 (s, 1H), 7.84 (s, 1H), 7.72 (s, 1H), 7.62 (d, J = 7.7 Hz, 1H), 7.58 (d, J = 7.9 Hz, 2H), 7.48 (t, J = 7.6 Hz, 1H), 7.42 (d, J = 7.5 Hz, 1H), 7.36–7.27 (m, 3H), 7.07 (t, J = 8.9 Hz, 1H), 5.25 (s, 2H), 2.59 (t, J = 7.6 Hz, 2H), 1.67–1.57 (m, 2H), 0.91 (t, J = 7.3 Hz, 3H); ^{13}C NMR (101 MHz, DMSO) δ 161.3, 153.1, 150.7, 149.3, 146.9, 142.8, 142.7, 141.7, 140.4, 137.2, 137.0, 129.2, 129.0, 126.5, 126.3, 126.0, 115.9, 111.0, 110.8, 70.8, 36.9, 24.0, 13.7. HRMS (ESI) calcd. for $C_{23}H_{21}F_2NO_2$ $[M + H]^+$, 382.1574, found 382.1624.

Synthesis of 3-((4′-butyl-[1,1′-biphenyl]-3-yl)methoxy)-2,6-difluorobenzamide (13): white solid, 88.3% yield; HPLC purity: 99.9%; ^{1}H NMR (500 MHz, DMSO) δ 8.12 (s, 1H), 7.84 (s, 1H), 7.72 (s, 1H), 7.62 (d, J = 7.7 Hz, 1H), 7.57 (d, J = 8.1 Hz, 2H), 7.48 (t, J = 7.6 Hz, 1H), 7.41 (d, J = 7.6 Hz, 1H), 7.35–7.27 (m, 3H), 7.07 (t, J = 8.4 Hz, 1H), 5.25 (s, 2H), 2.62 (t, J = 7.7 Hz, 2H), 1.62–1.54 (m, 2H), 1.37–1.28 (m, 2H), 0.91 (t, J = 7.4 Hz, 3H); ^{13}C NMR (101 MHz, DMSO) δ 161.3, 153.0, 150.7, 149.3, 146.9, 142.8, 142.7, 141.9, 140.4, 137.2, 137.0, 129.2, 128.9, 126.6, 126.3, 126.0, 115.9, 111.0, 110.8, 70.8, 34.4, 33.1, 21.8, 13.8. HRMS (ESI) calcd. for $C_{24}H_{23}F_2NO_2$ $[M + H]^+$, 396.1730, found 396.1782.

Synthesis of 2,6-difluoro-3-((4′-pentyl-[1,1′-biphenyl]-3-yl)methoxy)benzamide (14): white solid, 83.5% yield; HPLC purity: 99.8%; ^{1}H NMR (500 MHz, DMSO) δ 8.13 (s, 1H), 7.84 (s, 1H), 7.72 (s, 1H), 7.62 (d, J = 7.7 Hz, 1H), 7.57 (d, J = 8.0 Hz, 2H), 7.48 (t, J = 7.6 Hz, 1H), 7.42 (d, J = 7.5 Hz, 1H), 7.35–7.27 (m, 3H), 7.07 (t, J = 8.9 Hz, 1H), 5.25 (s, 2H), 2.61 (t, J = 7.6 Hz, 2H), 1.64–1.56 (m, 2H), 1.35–1.27 (m, 4H), 0.87 (t, J = 6.8 Hz, 3H); ^{13}C NMR (101 MHz, DMSO) δ 161.3, 153.1, 150.7, 149.3, 146.9, 142.8, 142.7, 141.9, 140.4, 137.2, 137.0, 129.2, 128.9, 126.6, 126.3, 126.0, 115.9, 111.0, 110.8, 70.8, 34.7, 30.9, 30.6, 22.0, 13.9. HRMS (ESI) calcd. for $C_{25}H_{25}F_2NO_2$ $[M + H]^+$, 410.1887, found 410.1938.

Synthesis of 2,6-difluoro-3-((4′-isopropyl-[1,1′-biphenyl]-3-yl)methoxy)benzamide (15): white solid, 83.3% yield; HPLC purity: 99.5%; ^{1}H NMR (500 MHz, DMSO) δ 8.13 (s, 1H), 7.84 (s, 1H), 7.72 (s, 1H), 7.64–7.56 (m, 3H), 7.48 (t, J = 7.6 Hz, 1H), 7.42 (d, J = 7.6 Hz, 1H), 7.37–7.29 (m, 3H), 7.07 (t, J = 8.9 Hz, 1H), 5.25 (s, 2H), 2.97–2.88 (m, 1H), 1.23 (d, J = 6.9 Hz, 6H); ^{13}C NMR (101 MHz, DMSO) δ 161.3, 153.1, 150.7, 149.3, 147.9, 146.9, 142.8, 140.4, 137.4, 137.0, 129.2, 126.9, 126.7, 126.6, 126.3, 126.0, 115.9, 111.0, 110.8, 70.8, 33.1, 23.8. HRMS (ESI) calcd. for $C_{23}H_{21}F_2NO_2$ $[M + H]^+$, 382.1574, found 382.1613.

Synthesis of 3-((4′-(tert-butyl)-[1,1′-biphenyl]-3-yl)methoxy)-2,6-difluorobenzamide (16): white solid, 81.8% yield; HPLC purity: 99.8%; ^{1}H NMR (500 MHz, DMSO) δ 8.13 (s, 1H), 7.84 (s, 1H), 7.72 (s, 1H), 7.64–7.57 (m, 3H), 7.49 (t, J = 7.6 Hz, 3H), 7.42 (d, J = 7.5 Hz, 1H), 7.36–7.29 (m, 1H), 7.07 (t, J = 8.9 Hz, 1H), 5.25 (s, 2H), 1.32 (s, 9H); ^{13}C NMR (101 MHz, DMSO) δ 161.3, 153.0, 150.7, 150.1, 149.3, 146.9, 142.8, 140.3, 137.0, 137.0, 129.2, 126.6, 126.4, 126.3, 126.0, 125.8, 115.9, 111.0, 110.8, 70.8, 34.3, 31.1. HRMS (ESI) calcd. for $C_{24}H_{23}F_2NO_2$ $[M + H]^+$, 396.1730, found 396.1773.

Synthesis of 2,6-difluoro-3-((4′-methoxy-[1,1′-biphenyl]-3-yl)methoxy)benzamide (17): white solid, 87.0% yield; HPLC purity: 100%; ^{1}H NMR (500 MHz, DMSO) δ 8.13 (s, 1H), 7.84 (s, 1H), 7.70 (s, 1H), 7.60 (t, J = 8.7 Hz, 3H), 7.46 (t, J = 7.6 Hz, 1H), 7.38 (d, J = 7.6 Hz, 1H), 7.35–7.29 (m, 1H), 7.10–7.02 (m, 3H), 5.24 (s, 2H), 3.80 (s, 3H); ^{13}C NMR (101

MHz, DMSO) δ161.3, 159.0, 153.1, 150.7, 149.3, 146.9, 142.8, 140.1, 137.0, 132.1,129.1, 127.8, 126.2, 126.0, 125.7, 115.9, 114.4, 110.0, 110.8, 70.9, 55.2. HRMS (ESI) calcd. for $C_{21}H_{17}F_2NO_3$ [M + H]$^+$, 370.1210, found 370.1236.

*Synthesis of 3-((4′-cyano-[1,1′-biphenyl]-*3-yl*)methoxy)-2,6-difluorobenzamide (**18**)*: white solid, 85.3% yield; HPLC purity: 100%; ^{1}H NMR (500 MHz, DMSO) δ 8.12 (s, 1H), 7.95 (d, *J* = 8.3 Hz, 2H), 7.89 (d, *J* = 8.3 Hz, 2H), 7.84 (s, 2H), 7.74 (d, *J* = 7.2 Hz, 1H), 7.58–7.51 (m, 2H), 7.37–7.29 (m, 1H), 7.07 (t, *J* = 8.6 Hz, 1H), 5.27 (s, 2H); ^{13}C NMR (101 MHz, DMSO) δ161.3, 153.1, 150.8, 146.8, 144.3, 142.7, 138.5, 137.4, 132.9,129.5, 128.2, 127.6, 126.9, 126.6, 118.8, 116.0, 115.9, 110.0, 110.8, 110.2, 70.9. HRMS (ESI) calcd. for $C_{21}H_{14}F_2N_2O_2$ [M + H]$^+$, 365.1057, found 365.1086.

*Synthesis of 2,6-difluoro-3-((4′-(trifluoromethyl)-[1,1′-biphenyl]-*3-yl*) methoxy)benzamide (**19**)*: white solid, 82.7% yield; HPLC purity: 99.1%; ^{1}H NMR (500 MHz, DMSO) δ 8.13 (s, 1H), 7.90 (d, *J* = 8.1 Hz, 2H), 7.83 (d, *J* = 8.0 Hz, 4H), 7.72 (d, *J* = 7.4 Hz, 1H), 7.59–7.49 (m, 2H), 7.38–7.30 (m, 1H), 7.07 (t, *J* = 8.7 Hz, 1H), 5.28 (s, 2H); ^{13}C NMR (101 MHz, DMSO) δ 161.3, 153.1, 150.7, 149.3, 146.9, 143.8, 142.8, 142.7, 138.8, 137.3, 129.4, 127.9, 127.5, 126.9, 126.5, 125.9, 125.8, 115.9, 111.1, 110.8, 70.7. HRMS (ESI) calcd. for $C_{21}H_{14}F_5NO_2$ [M + H]$^+$, 408.0978, found 408.1016.

*Synthesis of 2,6-difluoro-3-((4′-fluoro-[1,1′-biphenyl]-*3-yl*)methoxy) benzamide (**20**)*: white solid, 86.2% yield; HPLC purity: 100%; ^{1}H NMR (500 MHz, DMSO) δ 8.12 (s, 1H), 7.84 (s, 1H), 7.75–7.69 (m, 3H), 7.63 (d, *J* = 7.7 Hz, 1H), 7.50 (t, *J* = 7.6 Hz, 1H), 7.44 (d, *J* = 7.6 Hz, 1H), 7.35–7.28 (m, 3H), 7.07 (t, *J* = 8.9 Hz, 1H), 5.25 (s, 2H); ^{13}C NMR (101 MHz, DMSO) δ 163.2, 161.3, 160.8, 153.1, 150.7, 149.3, 146.9, 142.8, 139.4, 137.1, 136.3,129.2, 128.8, 126.9, 126.5, 126.2, 115.9, 111.0, 110.8, 70.8. HRMS (ESI) calcd. for $C_{20}H_{14}F_3NO_2$ [M + H]$^+$, 358.1010, found 358.1034.

*Synthesis of 3-((4′-chloro-[1,1′-biphenyl]-*3-yl*)methoxy)-2,6-difluorobenzamide (**21**)*: white solid, 81.1% yield; HPLC purity: 98.7%; ^{1}H NMR (500 MHz, DMSO) δ 8.13 (s, 1H), 7.84 (s, 1H), 7.75 (s, 1H), 7.70 (d, *J* = 8.4 Hz, 2H), 7.65 (d, *J* = 7.6 Hz, 1H), 7.55–7.44 (m, 4H), 7.37–7.28 (m, 1H), 7.07 (t, *J* = 8.8 Hz, 1H), 5.25 (s, 2H); ^{13}C NMR (101 MHz, DMSO) δ161.3, 153.1, 150.7, 149.3, 146.9, 142.7, 139.1, 138.6, 137.2,132.5, 129.3, 129.0, 128.5, 127.2, 126.5, 126.2, 116.0, 111.1, 110.8, 70.8. HRMS (ESI) calcd. for $C_{20}H_{14}ClF_2NO_2$ [M + H]$^+$, 374.0715, found 374.0760.

*Synthesis of 2,6-difluoro-3-((3′-fluoro-4′-(trifluoromethyl)-[1,1′-biphenyl]-*3-yl*)methoxy)benza-mide (**22**)*: white solid, 84.4% yield; HPLC purity: 99.8%; ^{1}H NMR (500 MHz, DMSO) δ 8.13 (s, 1H), 7.91–7.83 (m, 4H), 7.79–7.71 (m, 2H), 7.59–7.53 (m, 2H), 7.37–7.30 (m, 1H), 7.07 (t, *J* = 8.8 Hz, 1H), 5.27 (s, 2H); ^{13}C NMR (101 MHz, DMSO) δ161.3, 160.6, 158.1, 153.2, 150.8, 149.4, 146.8, 142.8, 137.4, 129.5, 128.5, 127.8, 127.0, 126.7, 123.1, 116.0, 115.3, 115.1, 111.1, 110.8, 70.6. HRMS (ESI) calcd. for $C_{21}H_{13}F_6NO_2$ [M + H]$^+$, 426.0884, found 426.0931.

*Synthesis of 3-((3′-chloro-4′-(trifluoromethyl)-[1,1′-biphenyl]-*3-yl*) methoxy)-2,6-difluorobenza- mide (**23**)*: white solid, 83.8% yield; HPLC purity: 98.6%; ^{1}H NMR (500 MHz, DMSO) δ 8.13 (s, 1H), 8.04 (s, 1H), 7.94 (d, *J* = 8.3 Hz, 1H), 7.91–7.81 (m, 3H), 7.77 (d, *J* = 3.6 Hz, 1H), 7.59–7.52 (m, 2H), 7.37–7.29 (m, 1H), 7.07 (t, *J* = 8.4 Hz, 1H), 5.27 (s, 2H); ^{13}C NMR (101 MHz, DMSO) δ161.3, 153.1, 150.7, 149.3, 146.9, 145.5, 142.7, 137.4, 137.2, 131.5, 129.5, 129.5, 128.5, 128.5, 127.1, 126.8, 125.8, 116.0, 111.1, 110.8, 70.7. HRMS (ESI) calcd. for $C_{21}H_{13}ClF_5NO_2$ [M + H]$^+$, 442.0589, found 442.0630.

*Synthesis of 2,6-difluoro-3-((2′-methoxy-4′-(trifluoromethyl)-[1,1′-biphenyl]-*3-yl*)methoxy)benza-mide (**24**)*: white solid, 86.5% yield; HPLC purity: 99.6%; ^{1}H NMR (500 MHz, DMSO) δ 8.13 (s, 1H), 7.84 (s, 1H), 7.59 (s, 1H), 7.53–7.44 (m, 4H), 7.39 (d, *J* = 6.5 Hz, 2H), 7.35–7.28 (m, 1H), 7.07 (t, *J* = 8.8 Hz, 1H), 5.24 (s, 2H), 3.85 (s, 3H); ^{13}C NMR (101 MHz, DMSO) δ161.3, 156.5, 153.1, 150.7, 149.3, 146.9, 142.8, 136.9, 136.3, 133.5, 131.2, 129.1, 128.7, 128.4, 127.2, 117.5, 115.9, 111.0, 110.8, 108.4, 70.7, 56.0. HRMS (ESI) calcd. for $C_{22}H_{16}F_5NO_3$ [M + H]$^+$, 438.1084, found 438.1140.

*Synthesis of 2,6-difluoro-3-((2′-methyl-4′-(trifluoromethyl)-[1,1′-biphenyl]-*3-yl*)methoxy)benza-mide (**25**)*: white solid, 81.4% yield; HPLC purity: 99.1%; ^{1}H NMR (500 MHz, DMSO) δ 8.12 (s, 1H), 7.84 (s, 1H), 7.69 (s, 1H), 7.62 (d, *J* = 8.0 Hz, 1H), 7.55–7.48 (m, 2H), 7.47–7.41 (m, 2H), 7.37 (d, *J* = 6.9 Hz, 1H), 7.35–7.28 (m, 1H), 7.07 (t, *J* = 8.4 Hz, 1H), 5.25 (s, 2H), 2.29 (s, 3H); ^{13}C NMR (101 MHz, DMSO) δ161.3, 153.2, 150.8, 149.4, 146.9, 145.0, 142.8, 140.0, 136.6, 136.4, 130.4, 128.7, 128.6, 128.3, 127.1, 126.9, 122.7, 116.1, 111.0, 110.8, 70.7, 56.0. HRMS (ESI) calcd. for $C_{22}H_{16}F_5NO_2$ [M + H]$^+$, 422.1135, found 422.1164.

*Synthesis of 3′-((3-carbamoyl-2,4-difluorophenoxy)methyl)-4-(trifluoromethyl)-[1,1′-biphenyl]-2- carboxamide (**26**)*: white solid, 87.5% yield; HPLC purity: 99.5%; ^{1}H NMR (500 MHz, DMSO) δ 8.13 (s, 1H), 7.93 (s, 1H), 7.86 (d, *J* = 9.1 Hz, 2H), 7.76 (s, 1H), 7.62 (d, *J* = 8.0 Hz, 1H), 7.56 (s, 1H), 7.53–7.43 (m, 4H), 7.36–7.28 (m, 1H), 7.08 (t, *J* = 8.8 Hz, 1H), 5.23 (s, 2H); ^{13}C NMR (101 MHz, DMSO) δ169.6, 161.3, 153.2, 150.8, 149.3, 146.9, 142.8, 142.6, 139.3, 138.0, 136.5, 131.1, 128.6, 128.2, 127.7, 127.4, 126.0, 124.3, 116.0, 111.0, 110.9, 70.8. HRMS (ESI) calcd. for $C_{22}H_{15}F_5N_2O_3$ [M + H]$^+$, 451.1036, found 451.1088.

*Synthesis of 3-((2′-chloro-4′-(trifluoromethyl)-[1,1′-biphenyl]-*3-yl*) methoxy)-2,6-difluorobenza- mide (**27**)*: white solid, 86.1% yield; HPLC purity: 98.2%; ^{1}H NMR (500 MHz, DMSO) δ 8.12 (s, 1H), 8.00 (s, 1H), 7.86–7.78 (m, 2H), 7.66 (d, *J* = 8.0 Hz, 1H), 7.59–7.53 (m, 3H), 7.49–7.45 (m, 1H), 7.35–7.29 (m, 1H), 7.07 (t, *J* = 8.9 Hz, 1H), 5.26 (s, 2H); ^{13}C NMR (101 MHz, DMSO) δ161.3, 153.1, 150.7, 149.4, 146.9, 143.6, 142.8, 137.6, 136.6, 132.5, 132.3, 128.9, 128.7, 128.5, 127.9, 126.8, 124.4, 116.0, 111.0, 110.8, 70.6. HRMS (ESI) calcd. for $C_{21}H_{13}ClF_5N_1O_2$ [M + H]$^+$, 442.0589, found 442.0635.

*Synthesis of 2,6-difluoro-3-((2′-fluoro-4′-(trifluoromethyl)-[1,1′-biphenyl]-*3-yl*)methoxy)benza-mide (**28**)*: white solid, 85.4% yield; HPLC purity: 99.5%; ^{1}H NMR (500 MHz, DMSO) δ 8.12 (s, 1H), 7.87–7.76 (m, 3H), 7.70 (d, *J* = 6.0 Hz, 2H), 7.62–7.54 (m, 3H), 7.36–7.30 (m, 1H), 7.07 (t, *J* = 8.9 Hz, 1H), 5.27 (s, 2H); ^{13}C NMR (101 MHz, DMSO) δ161.3, 160.0, 157.6, 153.2, 150.7, 149.3, 146.9, 142.8, 137.0, 133.9, 132.1, 129.1, 128.8, 128.2, 121.8, 115.9, 113.9, 113.7, 111.1, 110.8, 70.6. HRMS (ESI) calcd. for $C_{21}H_{13}F_6N_1O_2$ [M + H]$^+$, 426.0850, found 426.0850.

*Synthesis of 3-((2′,4′-bis(trifluoromethyl)-[1,1′-biphenyl]-*3-yl*) methoxy)-2,6-difluorobenzamide (**29**)*: white solid, 78.3% yield; HPLC purity: 98.6%; ^{1}H NMR (500 MHz, DMSO) δ 8.13 (d, *J* = 11.1 Hz, 3H), 7.84 (s, 1H), 7.68 (d, *J* = 7.9 Hz, 1H), 7.58–7.50 (m, 2H), 7.46 (s, 1H), 7.37–7.27 (m, 2H), 7.06 (t, *J* = 8.8 Hz, 1H), 5.25 (s, 2H); ^{13}C NMR (101 MHz, DMSO) δ161.3, 153.2, 150.8, 149.4, 146.9, 144.6, 142.7, 138.0, 136.4, 133.6, 129.2, 128.4, 128.3, 127.9, 127.8, 124.6, 123.1, 122.1, 116.0, 111.0, 110.8, 70.6. HRMS (ESI) calcd. for $C_{22}H_{13}F_8N_1O_2$ [M + H]$^+$, 476.0884, found 476.0933.

*Synthesis of 3-((4′-chloro-2′-methyl-[1,1′-biphenyl]-*3-yl*)methoxy)-2,6-difluorobenzamide (**30**)*: white solid, 73.3% yield; HPLC purity: 99.2%; ^{1}H NMR (500 MHz, DMSO) δ 8.12 (s, 1H), 7.84 (s, 1H), 7.51–7.44 (m, 2H), 7.41 (s, 2H), 7.35–7.28 (m, 3H), 7.22 (d, *J* = 8.2 Hz, 1H), 7.07 (t, *J* = 8.8 Hz, 1H), 5.24 (s, 2H), 2.21 (s, 3H); ^{13}C NMR (101 MHz, DMSO) δ161.3, 153.2, 150.8, 149.3, 146.9, 142.8, 140.2, 139.8, 137.4, 136.5, 132.0, 131.2, 129.9, 128.7, 128.4, 126.8, 125.9, 116.0, 111.0, 70.7, 20.0. HRMS (ESI) calcd. for $C_{21}H_{16}ClF_2N_1O_2$ [M + H]$^+$, 388.0871, found 388.0893.

*Synthesis of 3-((2′,4′-dichloro-[1,1′-biphenyl]-*3-yl*)methoxy)-2,6-difluorobenzamide (**31**)*: white solid, 84.5% yield; HPLC purity: 96.2%; ^{1}H NMR (500 MHz, DMSO) δ 8.12 (s, 1H), 7.85 (s, 1H), 7.75 (s, 1H), 7.57–7.49 (m, 4H), 7.48–7.38 (m, 2H), 7.35–7.28 (m, 1H), 7.07 (t, *J* = 8.8 Hz, 1H), 5.25 (s, 2H); ^{13}C NMR (101 MHz, DMSO) δ161.3, 153.1, 150.8, 149.3, 142.8, 138.4, 137.8, 136.5, 133.1, 132.7, 132.3, 129.3, 129.0, 128.7, 127.7, 127.5, 115.9, 111.1, 110.8, 70.6. HRMS (ESI) calcd. for $C_{20}H_{13}Cl_2F_2N_1O_2$ [M + H]$^+$, 408.0325, found 408.0352.

*Synthesis of 3-((4′-chloro-2′-fluoro-[1,1′-biphenyl]-*3-yl*)methoxy)-2,6-difluorobenzamide (**32**)*: white solid, 81.3% yield; HPLC purity: 97.6%; ^{1}H NMR (500 MHz, DMSO) δ 8.14 (s, 1H), 7.86 (s, 1H), 7.63 (s, 1H),

7.61–7.48 (m, 5H), 7.41 (d, $J = 8.2$ Hz, 1H), 7.36–7.29 (m, 1H), 7.07 (t, $J = 8.8$ Hz, 1H), 5.25 (s, 2H). ^{13}C NMR (101 MHz, DMSO) δ161.3, 160.2, 157.7, 153.2, 149.3, 142.8, 136.9, 134.2, 132.0, 129.0, 128.6, 128.2, 127.6, 125.3, 116.9, 116.6, 115.9, 111.1, 110.8, 70.6. HRMS (ESI) calcd. for $C_{20}H_{13}ClF_3N_1O_2$ $[M + H]^+$, 392.0620, found 392.0658.

Synthesis of 3-((4′-chloro-2'-(trifluoromethyl)-[1,1′-biphenyl]-3-yl) methoxy)-2,6-difluoroben- zamide ***(33)***: white solid, 79.2% yield; HPLC purity: 95.7%; ^{1}H NMR (500 MHz, DMSO) δ 8.12 (s, 1H), 7.91 (s, 1H), 7.88–7.79 (m, 2H), 7.55–7.47 (m, 2H), 7.45 (d, $J = 8.2$ Hz, 1H), 7.41 (s, 1H), 7.29 (t, $J = 9.8$ Hz, 2H), 7.06 (t, $J = 8.9$ Hz, 1H), 5.23 (s, 2H); ^{13}C NMR (101 MHz, DMSO) δ161.3, 153.2, 150.8, 146.9, 142.8, 139.2, 138.2, 136.3, 134.1, 132.9, 132.3, 128.5, 128.4, 128.0, 127.5, 126.1, 121.8, 116.0, 111.0, 110.8, 70.6. HRMS (ESI) calcd. for $C_{21}H_{13}ClF_5N_1O_2$ $[M + H]^+$, 442.0589, found 442.0633.

5.1.4. Methyl 5-chloro-4'-(trifluoromethyl)-[1,1′-biphenyl]-3-carboxylate (38)

To a solution of methyl 3-bromo-5-chlorobenzoate **36** (301.6 mg, 1.22 mmol) in dioxane (6 mL) and H_2O (1 mL) was added (4-(trifluoromethyl)phenyl)boronic acid **37** (300.5 mg, 1.58 mmol), Pd(dppf)Cl_2 (187.5 mg, 0.26 mmol), Na_2CO_3 (429.4 mg, 4.05 mmol) and heated with microwave at 100 °C for 1 h. The reaction mixture was diluted with EtOAc (25 mL), washed with H_2O, washed with brine, dried over Na_2SO_4. The resulting solution was evaporated and purified by flash column chromatography (PE/EA, 97/3) to afford the intermediate **38** (370 mg, 96.2%) as a light yellow oil. ^{1}H NMR (500 MHz, DMSO) δ 8.17–8.14 (m, 1H), 8.06–8.03 (m, 1H), 7.76 (t, $J = 1.7$ Hz, 1H), 7.71 (q, $J = 8.5$ Hz, 4H), 3.96 (s, 3H). ESI-MS calcd. for $C_{15}H_{10}ClF_3O_2$ $[M + H]^+$, 315.0, found 315.1.

5.1.5. (5-chloro-4'-(trifluoromethyl)-[1,1′-biphenyl]-3-yl)methanol (39)

To a solution of **38** (370 mg, 1.18 mmol) in THF (8 mL) was added $LiAlH_4$ in THF solution (0.52 mL, 2.5 M, 1.3 mmol) at 0 °C for 2 h. The reaction mixture was quenched with $Na_2SO_4{\cdot}10H_2O$ (419 mg, 1.3 mmol), filtered and washed with EA (80 mL). The filtrate was evaporated and purified by flash column chromatography (PE/EA, 91/9) to afford the intermediate **39** (260 mg, 77.1%) as a white solid. ^{1}H NMR (500 MHz, DMSO) δ 7.69 (q, $J = 8.4$ Hz, 4H), 7.48 (d, $J = 11.3$ Hz, 2H), 7.40 (s, 1H), 4.77 (s, 2H). ESI-MS calcd. for $C_{15}H_{10}ClF_3O_2$ $[M + H]^+$, 287.0, found 287.1.

5.1.6. 2,6-Difluoro-3-(2-hydroxy-1-(4'-(trifluoromethyl)-[1,1′-biphenyl]-3-yl)ethoxy)benzamide (19a)

White solid, 72.3% yield; HPLC purity: 99.1%; ^{1}H NMR (500 MHz, DMSO) δ 8.12 (s, 1H), 7.89 (d, $J = 8.0$ Hz, 2H), 7.83 (d, $J = 7.2$ Hz, 3H), 7.79 (s, 1H), 7.66 (d, $J = 7.4$ Hz, 1H), 7.52–7.44 (m, 2H), 7.21–7.13 (m, 1H), 6.94 (t, $J = 8.8$ Hz, 1H), 5.47 (s, 1H), 5.23 (d, $J = 5.5$ Hz, 1H), 3.90–3.82 (m, 1H), 3.75–3.68 (m, 1H); ^{13}C NMR (101 MHz, DMSO) δ161.4, 153.0, 150.6, 149.6, 147.2, 143.9, 142.3, 139.2, 138.7, 129.4, 128.2, 127.9, 127.6, 126.8, 125.8, 125.6, 123.0, 117.1, 110.9, 110.7, 82.3, 65.5. HRMS (ESI) calcd. for $C_{21}H_{13}ClF_5N_1O_2$ $[M + H]^+$, 442.0589, found 442.0630.

5.1.7. Synthesis of 3-((5-chloro-4'-(trifluoromethyl)-[1,1′-biphenyl]-3-yl) methoxy)-2,6-difluorobenza- mide (19b)

White solid, 78.8% yield; HPLC purity: 99.4%; ^{1}H NMR (500 MHz, DMSO) δ 8.14 (s, 1H), 7.94 (d, $J = 8.1$ Hz, 2H), 7.84 (d, $J = 8.2$ Hz, 3H), 7.81 (d, $J = 5.5$ Hz, 2H), 7.59 (s, 1H), 7.37–7.30 (m, 1H), 7.09 (t, $J = 8.9$ Hz, 1H), 5.28 (s, 2H); ^{13}C NMR (101 MHz, DMSO) δ161.3, 153.3, 150.9, 149.3, 146.9, 142.6, 142.3, 140.9, 139.7, 134.1, 128.7, 127.8, 127.3, 126.6, 126.0, 125.9, 125.2, 116.0, 111.2, 110.9, 69.9. HRMS (ESI) calcd. for $C_{22}H_{16}F_5N_1O_3$ $[M + H]^+$, 438.1084, found 438.1127.

5.1.8. Synthesis of 3-(1-(4′-chloro-2′-methyl-[1,1′-biphenyl]-3-yl)-2-hydroxyethoxy)-2,6-difluoro- benzamide (30a)

White solid, 98.5% yield; HPLC purity: 99.4%; ^{1}H NMR (500 MHz, DMSO) δ 8.12 (s, 1H), 7.83 (s, 1H), 7.46–7.37 (m, 4H), 7.31 (d, $J = 8.2$ Hz, 1H), 7.26 (d, $J = 6.9$ Hz, 1H), 7.21 (d, $J = 8.2$ Hz, 1H), 7.19–7.13 (m, 1H), 6.95 (t, $J = 8.9$ Hz, 1H), 5.47–5.42 (m, 1H), 5.23 (t, $J = 5.3$ Hz, 1H), 3.88–3.81 (m, 1H), 3.74–3.67 (m, 1H), 2.17 (s, 3H); ^{13}C NMR (101 MHz, DMSO) δ161.8, 153.5, 151.1, 150.1, 147.6, 142.7, 140.4, 140.2, 138.7, 137.9, 132.4, 131.7, 130.4, 129.1, 128.0, 126.4, 126.0, 117.7, 111.4, 82.6, 65.9, 20.4. HRMS (ESI) calcd. for $C_{22}H_{18}ClF_2NO_3$ $[M + H]^+$, 418.0977, found 418.1001.

5.2. Determination of the minimal inhibitory concentration (MIC)

The minimum inhibitory concentration (MIC) of the synthesized compounds was conducted in the 96-well microplate using the broth microdilution method described in the Clinical and Laboratory Standards Institute (CLSI) guidelines [22]. The Log-phase bacteria strains cultured in Mueller Hinton broth (MHB) were diluted and added to 96-well microtiter plates containing 2-fold serial dilutions of compound or control drug at concentrations ranging from 128 to 0.25 μg/mL or 2 to 0.004 μg/mL. The final volume in each well was 0.1 mL and the microtiter plates were incubated aerobically for 18 h at 37 °C. The absorbance at 600 nm (OD600) was recorded and the MIC was defined as the lowest compound concentration at which the growth of bacteria was inhibited by ≥ 90%. Three independent assays were performed for each test.

5.3. Cytotoxicity assay

The active newly synthesized compounds were screened for their cytotoxicity against Vero cells using Alamar blue assay. ~2×10^3 cells/well was seeded in 96 well plate and incubated at 37 °C with a 5% CO_2 atmosphere. After 24 h, compounds were added and incubated for 72 h at 37 °C with 5% CO_2 atmosphere. After the incubation period, cells were incubated with AlamarBlue™ Cell Viability Reagent at 1: 10 dilution (v/v) in dark for 3 h and the absorbance was measured at Ex/Em: 560/590 nm.

5.4. Minimum bactericidal concentration (MBC) assay

MBC assay was conducted using the broth microdilution assay described in the preceding section. After the 24 h incubation period, 5-μL aliquots from the clear solution of microtiter wells were plated onto LB agar plate. Then the LB agar plates were incubated aerobically at 37 °C for 24 h and the colonies were counted. The MBC value is being defined as the lowest compound concentration that no colonies were observed on the LB agar plate.

5.5. Time-kill curve assay

The log-phase culture of *S. aureus* ATCC25923 and *Bacillus* ATCC9372 were diluted to approximately 10^6 CFU/mL in volumes of MHB, containing various concentrations of **30** (1 × , 2 × , 4 × and 8 × MIC) or vancomycin (2 × MIC). Cultures were incubated at 37 °C with shaking. At appropriate time intervals (3, 6, 12 and 24 h), 100 μL samples were removed for serial dilution in 900 μL volumes of MHB and 100 μL volumes from three dilutions were spread onto LB agar plate. All LB agar plates were incubated at 37 °C and the cell counts (CFU/mL) were enumerated after incubating the plates at 37 °C after 24 h.

5.6. Drug resistance study

The initial MIC values of compound **30** and control antibiotic (norfloxacin) against *S. aureus* ATCC29213 were determined as described above. Bacteria from duplicate test tubes at a concentration of 0.5 × MIC were used to prepare the bacterial dilution (approximately 5×10^5 CFU/mL) for the next MIC assay. Then, these bacterial suspensions were incubated with compound **30** and norfloxacin. After incubation at 35 °C

for 24 h, the fold increase in MIC value was determined. The process was repeated for 18 passages.

5.7. Transmission electron microscopy (TEM)

Recombinant *Sa*FtsZ protein was purchased from Cytoskeleton (FTZ02). At room temperature, *Sa*FtsZ (12 μM) was incubated in 50 mM Hepes-KOH buffer (pH 6.8) in the presence of the test compound dissolved in DMSO for 10 min. Then 50 mM KCl, 5 mM $MgCl_2$ and 1 mM GTP were added to reaction and incubated at 37 °C for 20 min. After that, 10-μL drops of the resulting dilutions were placed on glow-discharged, copper, 400 mesh, Formvar/carbon-coated grids. The grids were negatively stained with a solution of 1% phosphotungstic acid for 1 min and air-dried. The grids were then digitally imaged on a Tecnai G2 Spirit transmission microscope [26].

5.8. FtsZ polymerization assay

The polymerization of *Sa*FtsZ protein was monitored using a microtiter plate-based light-scattering (turbidity) assay [18,26]. in which changes in light scattering are reflected by corresponding changes in absorbance at 340 nm. Test compound were combined with 1 mM GTP and 12 μM FtsZ in 100 μL of reaction solution, which contained 50 mM Hepes, 50 mM KCl and 5 mM $MgCl_2$. Reactions were assembled in half-volume, flat-bottom microtiter plates, and polymerization was continuously monitored at 25 °C by measuring A340 in a BioTek Instruments Cytation 5 plate reader.

5.9. GTPase activity test

The GTPase activity of *Sa*FtsZ was measured by using an ATPase/GTPase Activity Assay Kit (SIGMA MAK113) according to the Kit instructions [27,28]. FtsZ (6 μM) was preincubated with different concentrations of tested compounds in 50 mM Hepes-KOH buffer for 10 min at room temperature. Then 300 mM of KCl, 5 mM of $MgCl_2$ and 1 mM GTP were added. The reaction mixture was incubated at 37 °C. After 30 min, the reactions were quenched by adding 100 mL of Cytophos reagent for 10 min. Inorganic phosphate was quantified by measuring the absorbance at 620 nm with a microplate reader (BioTek Instruments Ltd, US).

5.10. Visualization of bacterial morphology

Phenotype assay was performed essentially as described previously [15,18,25,29–31]. Briefly, the *Bacillus* ATCC9372 cells were grown overnight in MH broth at 37 °C. The cultures were diluted to an OD600 of approximately 0.01 and 10 μL aliquots were added to transparent 96-well microtiter microplates containing dilutions of compound in 100-μL volumes of medium. After incubation for approximately 3 h at 37 °C, the cells for morphology studies were harvested and resuspended in 100 μL of PBS buffer containing 0.2% agarose. After that, 8 μL of the suspension mixture was then placed on a microscopic slide. The morphology of the bacterial cells was observed and captured under a Nikon Eclipse Ti2 Inverted Microscope at 100 magnifications.

5.11. Computational study and molecular dynamics

Docking studies were performed using induced fit docking (IFD) module of Schrödinger [29]. The crystal structure of FtsZ (PDB ID: 3vob) was downloaded from the Protein Data Bank (PDB). Protein-ligand interactions and binding poses of ligands were visualized and analyzed using Pymol. MD simulations were carried out with Amber 20, and the force field parameter of the complex system was built with TLEAP package and Amber ff14SB [32].

5.12. Microsome stability experiment

This experiment was conducted by ChemPartner. Briefly, the metabolic stability assay in mouse, rat and human liver microsomes were determined by measuring the percentage of compound remaining after incubation. The assay incubation system contained microsomes with final liver microsomal protein concentration of 0.75 mg/mL, 0.5 mM compound and NADPH regeneration system (6 mM) in 100 mM phosphate buffer at pH 7.4. Firstly, all the plates with microsome and compound were pre-incubate at 37 °C for 5 min. Then 15 μL of NADPH stock solution (6 mM) was added to the plates to start the reaction and timing. At 5-min, 15-min, 30-min, and 45- min, 135 μL of ACN containing IS was added to the wells of corresponding plates, respectively, to stop the reaction. After quenching, shake the plates at the vibrator (IKA, MTS 2/4) for 10 min (600 rpm/min) and then centrifuge at 5594 g for 15 min (Thermo Multifuge × 3R). Finally, transfer 50 μL of the supernatant from each well into a 96-well sample plate containing 50 mL of ultrapure water (Millipore, ZMQS50F01) for LC/MS analysis.

5.13. Pharmacokinetics

Male ICR mice were used in the PK study of compound **30**. The dosage and the number of animals for each group were presented in Table 5. Both the intravenous and oral doses were formulated in a solution of 5% DMSO, 4% ethanol, 5% Cremophor EL and 86% water. The time points for blood sample collection were 15 min, 30 min, 1 h, 2 h, 4 h, 6 h, 8 h and 24 h after dosing for oral administration, and 5 min, 15 min, 30 min, 1 h, 2 h, 4 h, 8 h and 24 h for intravenous injection. The plasma samples were collected, centrifuged and stored at -20 °C till the analysis. The concentration of the tested compound in plasma was determined with LC-MS/MS 18 (TQ6500, Triple quad). The PK parameters were calculated with WinNonlin software V6.3 using non-compartmental analysis (Pharsight Corporation, Mountain Vew, USA)

5.14. In vivo efficacy

All experimental procedures conformed to the animal experiment guidelines of the Animal Care and Welfare Committee of Bioland Laboratory. The cultures of *S. aureus* ATCC25923 in mid-log phase were centrifuged, and the cell pellets were suspended and diluted in sterile saline solution. Groups of ICR mouse with an average weight of 25 g were injected intravenously with 0.1 mL of saline solution containing *S. aureus* ATCC25923 of 6×10^7 CFU/mL. After 1 h, the mice were then intraperitoneal administered with 0.5 mL saline, 0.5 mL compound **30** (25 mg/kg), and 0.5 mL vancomycin (25 mg/kg), respectively. To evaluate bacteremia, eye blood samples were obtained before treatment and 1 h after treatment, and then plated onto the agar plates. At last, the plates were incubated at 37 °C overnight for CFU enumeration [18].

Declaration of competing interest

The authors declare that they have no known competing financial interests or personal relationships that could have appeared to influence the work reported in this paper.

Acknowledgements

This work was supported by GuangDong Basic and Applied Basic Research Foundation (No. 2020A1515110430); The authors also thank the Bioland Laboratory for financial support.

Appendix A. Supplementary data

Supplementary data to this article can be found online at https://doi.org/10.1016/j.ejmech.2022.114553.

References

[1] D.M. De Oliveira, B.M. Forde, T.J. Kidd, P.N. Harris, M.A. Schembri, S.A. Beatson, D.L. Paterson, M.J. Walker, Antimicrobial resistance in ESKAPE pathogens, Clin. Microbiol. Rev. 33 (2020) e00181-00119.

[2] S.S. Boswihi, E.E. Udo, Methicillin-resistant Staphylococcus aureus: an update on the epidemiology, treatment options and infection control, Curr. Med. Res. Practice. 8 (2018) 18–24.

[3] T. den Blaauwen, L.W. Hamoen, P.A. Levin, The divisome at 25: the road ahead, Curr. Opin. Microbiol. 36 (2017) 85–94.

[4] R.L. Lock, E.J. Harry, Cell-division inhibitors: new insights for future antibiotics, Nat. Rev. Drug Discov. 7 (2008) 324–338.

[5] D.W. Adams, J. Errington, Bacterial cell division: assembly, maintenance and disassembly of the Z ring, Nat. Rev. Microbiol. 7 (2009) 642–653.

[6] R. McQuillen, J. Xiao, Insights into the structure, function, and dynamics of the bacterial cytokinetic FtsZ-ring, Annu. Rev. Biophys. 49 (2020) 309–341.

[7] M. Wang, C. Fang, B. Ma, X. Luo, Z. Hou, Regulation of cytokinesis: FtsZ and its accessory proteins, Curr. Genet. 66 (2020) 43–49.

[8] B. Beall, J. Lutkenhaus, FtsZ in Bacillus subtilis is required for vegetative septation and for asymmetric septation during sporulation, Genes Dev. 5 (1991) 447–455.

[9] K.D. Kusuma, M. Payne, A.T. Ung, A.L. Bottomley, E.J. Harry, FtsZ as an antibacterial target: status and guidelines for progressing this avenue, ACS Infect. Dis. 5 (2019) 1279–1294.

[10] N. Silber, C.L. Matos de Opitz, C. Mayer, P. Sass, Cell division protein FtsZ: from structure and mechanism to antibiotic target, Future Microbiol. 15 (2020) 801–831.

[11] S. Tripathy, S.K. Sahu, FtsZ inhibitors as a new genera of antibacterial agents, Bioorg. Chem. 91 (2019), 103169.

[12] G. Chiodini, M. Pallavicini, C. Zanotto, M. Bissa, A. Radaelli, V. Straniero, C. Bolchi, L. Fumagalli, P. Ruggeri, C.D.G. Morghen, Benzodioxane–benzamides as new bacterial cell division inhibitors, Eur. J. Med. Chem. 89 (2015) 252–265.

[13] L.G. Czaplewski, I. Collins, E.A. Boyd, D. Brown, S.P. East, M. Gardiner, R. Fletcher, D.J. Haydon, V. Henstock, P. Ingram, Antibacterial alkoxybenzamide inhibitors of the essential bacterial cell division protein FtsZ, Bioorg. Med. Chem. Lett 19 (2009) 524–527.

[14] P. Domadia, S. Swarup, A. Bhunia, J. Sivaraman, D. Dasgupta, Inhibition of bacterial cell division protein FtsZ by cinnamaldehyde, Biochem. Pharmacol. 74 (2007) 831–840.

[15] D.J. Haydon, N.R. Stokes, R. Ure, G. Galbraith, J.M. Bennett, D.R. Brown, P. J. Baker, V.V. Barynin, D.W. Rice, S.E. Sedelnikova, An inhibitor of FtsZ with potent and selective anti-staphylococcal activity, Science 321 (2008) 1673–1675.

[16] T. Läppchen, V.A. Pinas, A.F. Hartog, G.-J. Koomen, C. Schaffner-Barbero, J. M. Andreu, D. Trambaiolo, J. Löwe, A. Juhem, A.V. Popov, Probing FtsZ and tubulin with C8-substituted GTP analogs reveals differences in their nucleotide binding sites, Chem. Biol. 15 (2008) 189–199.

[17] V. Straniero, M. Pallavicini, G. Chiodini, C. Zanotto, L. Volontè, A. Radaelli, C. Bolchi, L. Fumagalli, M. Sanguinetti, G. Menchinelli, 3-(Benzodioxan-2-ylmethoxy)-2, 6-difluorobenzamides bearing hydrophobic substituents at the 7-position of the benzodioxane nucleus potently inhibit methicillin-resistant Sa and Mtb cell division, Eur. J. Med. Chem. 120 (2016) 227–243.

[18] F. Bi, D. Song, N. Zhang, Z. Liu, X. Gu, C. Hu, X. Cai, H. Venter, S. Ma, Design, synthesis and structure-based optimization of novel isoxazole-containing benzamide derivatives as FtsZ modulators, Eur. J. Med. Chem. 159 (2018) 90–103.

[19] H. Lu, Q. Zhou, J. He, Z. Jiang, C. Peng, R. Tong, J. Shi, Recent advances in the development of protein–protein interactions modulators: mechanisms and clinical trials, Signal Transduct. Targeted Ther. 5 (2020) 1–23.

[20] S. Qiang, C. Wang, H. Venter, X. Li, Y. Wang, L. Guo, R. Ma, S. Ma, Synthesis and biological evaluation of novel FtsZ-targeted 3-arylalkoxy-2, 6-difluorobenzamides as potential antimicrobial agents, Chem. Biol. Drug Des. 87 (2016) 257–264.

[21] T. Matsui, J. Yamane, N. Mogi, H. Yamaguchi, H. Takemoto, M. Yao, I. Tanaka, Structural reorganization of the bacterial cell-division protein FtsZ from Staphylococcus aureus, Acta Crystallogr. Sect. D Biol. Crystallogr. 68 (2012) 1175–1188.

[22] V. Straniero, C. Zanotto, L. Straniero, A. Casiraghi, S. Duga, A. Radaelli, C. De Giuli Morghen, E. Valoti, 2,6-Difluorobenzamide inhibitors of bacterial cell division protein FtsZ: design, synthesis, and structure-activity relationships, ChemMedChem 12 (2017) 1303–1318.

[23] N.R. Stokes, N. Baker, J.M. Bennett, P.K. Chauhan, I. Collins, D.T. Davies, M. Gavade, D. Kumar, P. Lancett, R. Macdonald, Design, synthesis and structure–activity relationships of substituted oxazole–benzamide antibacterial inhibitors of FtsZ, Bioorg. Med. Chem. Lett 24 (2014) 353–359.

[24] E. Ferrer-González, J. Fujita, T. Yoshizawa, J.M. Nelson, A.J. Pilch, E. Hillman, M. Ozawa, N. Kuroda, H.M. Al-Tameemi, J.M. Boyd, Structure-Guided Design of a fluorescent probe for the Visualization of ftsZ in clinically important Gram-positive and Gram-negative Bacterial pathogens, Sci. Rep. 9 (2019) 1–16.

[25] N.R. Stokes, J.r. Sievers, S. Barker, J.M. Bennett, D.R. Brown, I. Collins, V. M. Errington, D. Foulger, M. Hall, R. Halsey, Novel inhibitors of bacterial cytokinesis identified by a cell-based antibiotic screening assay, J. Biol. Chem. 280 (2005) 39709–39715.

[26] C.-C. Chen, Y.-Q. Zhang, D.-X. Zhong, X.-H. Huang, Y.-H. Zhang, W.-H. Jiang, M. Li, Q. Chen, W.-L. Wong, Y.-J. Lu, The study of 9, 10-dihydroacridine derivatives as a new and effective molecular scaffold for antibacterial agent development, Biochem. Biophys. Res. Commun. 546 (2021) 40–45.

[27] J.M. Andreu, C. Schaffner-Barbero, S. Huecas, D. Alonso, M.L. Lopez-Rodriguez, L. B. Ruiz-Avila, R. Núñez-Ramírez, O. Llorca, A.J. Martín-Galiano, The antibacterial cell division inhibitor PC190723 is an FtsZ polymer-stabilizing agent that induces filament assembly and condensation, J. Biol. Chem. 285 (2010) 14239–14246.

[28] S. Cai, W. Yuan, Y. Li, X. Huang, Q. Guo, Z. Tang, Z. Fang, H. Lin, W.-L. Wong, K.-Y. Wong, Antibacterial activity of indolyl-quinolinium derivatives and study their mode of action, Bioorg. Med. Chem. 27 (2019) 1274–1282.

[29] N.R. Stokes, N. Baker, J.M. Bennett, J. Berry, I. Collins, L.G. Czaplewski, A. Logan, R. Macdonald, L. MacLeod, H. Peasley, An improved small-molecule inhibitor of FtsZ with superior in vitro potency, drug-like properties, and in vivo efficacy, Antimicrob. Agents Chemother. 57 (2013) 317–325.

[30] N. Sun, R.-L. Du, Y.-Y. Zheng, B.-H. Huang, Q. Guo, R.-F. Zhang, K.-Y. Wong, Y.-J. Lu, Antibacterial activity of N-methylbenzofuro [3, 2-b] quinoline and N-methylbenzoindolo [3, 2-b]-quinoline derivatives and study of their mode of action, Eur. J. Med. Chem. 135 (2017) 1–11.

[31] Z. Fang, S. Zheng, K.-F. Chan, W. Yuan, Q. Guo, W. Wu, H.-K. Lui, Y. Lu, Y.-C. Leung, T.-H. Chan, Design, synthesis and antibacterial evaluation of 2, 4-disubstituted-6-thiophenyl-pyrimidines, Eur. J. Med. Chem. 161 (2019) 141–153.

[32] J.A. Maier, C. Martinez, K. Kasavajhala, L. Wickstrom, K.E. Hauser, C. Simmerling, ff14SB: improving the accuracy of protein side chain and backbone parameters from ff99SB, J. Chem. Theor. Comput. 11 (2015) 3696–3713.